Integrated Master in Chemical Engineering

Synthesis of Peptide-based Porous Materials

Master's Thesis

by

Seyedali Emami

Supervisor: **Prof. Adélio Mendes**
Co-Supervisor: **Prof. Luis Gales**

Universidade do Porto
Faculdade de Engenharia
FEUP

Department of Chemical Engineering

July 2013

"از سخن عشق ندیدم خوش تر   یادگاری که در این گنبد دوار بماند"

حافظ

"I have never seen a more beautiful reminder

Than the words of love that linger in this turning dome"

-Hafez (1325-1389 C.E.)

Acknowledgments

Abstract

Metal organic frameworks attract significant attention during the last decades, due to their wide range application in gas storage, adsorption, and drug delivery. In this work, we synthesized two new metal-peptide frameworks (MPF) through assembling GlyAsp dipeptide with Zn(II) and Co(II) metal ions. The structures of Zn and Co porous frameworks exhibited two-dimensional and three-dimensional topologies, respectively. In fact, cobalt-based framework is among the few examples of reported MPFs, which has a 3-D structure. Thermogravimetric analysis of these compounds showed thermal stability up to 250 $^{\circ}$C, which is a decent stability compared to materials with similar structure.

Keywords:

Resumo

As estruturas de materiais híbridos metal-orgânico têm atraído uma atenção significativa nas últimas décadas, devido à sua ampla gama de aplicações que vão desde a concentração/separação de gases por adsorção à utlização como veículos para transporte de fármacos. Neste trabalho, sintetizou-se duas novas estruturas de metal-peptídeo (MPF) através da combinação do dipéptido GlyAsp com Zn(II) e Co(II). As estruturas exibem tipologias bidimensionais e tridimensionais, respetivamente. Na verdade, a estrutura de base de cobalto é um dos poucos exemplos de MPFs reportados, que tem uma estrutura 3-D. A análise termogravimétrica destes compostos mostrou uma estabilidade térmica superior à da maior parte dos materiais desta classe, e que se situa acima dos 250 ^{o}C.

Declaration

I, **Seyedali Emami**, do hereby declare that, this thesis is entirely my original work. Others sources of information have been duly acknowledged and referenced.

Seyedali Emami

July 2013, Porto

Contents

Nomenclature

Symbol	Description	Default Unit
t	time	s
P	pressure	bar
V	volume	cm^3
m	mass	g
ρ	density	$g.cm^{-1}$
M_w	molecular weight	$g.mol^{-1}$
n	molar number	mol
R	gas constant	$cm^3.bar.K^{-1}.mmol^{-1}$
n_{ads}	molar number adsorbed	mmol
T	temperature	K
q	adsorption uptake	$mol.kg^{-1}$

Acronyms and Abbreviations

AA	Amino Acid
Ac	Acetyl
Ala	Alanine
Arg	Arginine
Asp	Aspartic acid
BDC	1,4-benzenedicarboxylic acid
BDC-(OH)$_2$	2,5-dihydroxybenzenedicarboxylate
BPB	1,2-bis(4'-pyrazolyl)benzene
BPE	1,2-bis(4-pyridyl)-ethane
BTC	1,3,5-benzentricarbozylate
DMF	Dimethylformamide
DPNI	N,N'-di-(4-pyridyl)-1,4,5,8-naphthalene tetracarboxydimiimide
DSCP	c,c,t-Pt(NH$_3$)$_2$Cl$_2$(OOCCH$_2$CH$_2$CO$_2$H)$_2$
EDS	Energy Dispersive Spectrometry
Glu	Glutamate
Gly	Glycine
HEPES	4-(2-hydroxyethyl)-1-piperazineethanesulfonic acid
HKUST	Hong Kong University of Science and Technology
IBU	Ibuprofen
INA	Isonicotinic acid
IUPAC	International Union of Pure and Applied Chemistry
MBioF	Metal-biomolecule Framework
MEA	Membrane Electrode Assembly
MIL	Materials of Institut Lavoisier
MOF	Metal-organic Framework
MPF	Metal-peptide Framework
NCP	Nanoscale Coordination Polymer
NDC	2,6-naphthalendicarboxylate
ORR	Oxygen Reduction Reaction

PEM	Proton Exchange Membrane
PSA	Pressure Swing Adsorption
SBU	Secondary Building Unit
SEM	Scanning Electron Microscope
TEOS	Tetraethyl orthosilicate
TG	Thermogravimetric
TGA	Thermogravimetric Analysis
Thr	Threonine
TSA	Thermal Swing Adsorption
WDS	Wavelength Dispersive Spectrometry
XRPD	X-Ray Powder Diffraction
ZIF	Zeolitic Imidazolate Framework

List of Figures

List of Tables

Chapter 1

1.   Metal-organic framework

1.1. Introduction

Metal-organic frameworks (MOFs) are classified as hybrid materials, which are formed in the most elementary sense by connecting together, metal ions with polytopic organic linkers often resulting in two- or three-dimensional periodic structures. MOFs could be called with other names such as, porous coordination networks, porous coordination polymers, etc. Generally, MOFs are named according to their type of framework and the researchers who constructed it [1].

A hallmark property of MOFs is their intrinsic porosity, which makes them very useful in gas storage, drug storage and delivery, adsorption, separation, electrochemical and catalysis. These characteristics make MOFs one of the most exciting and rapidly growing areas of modern chemistry research [2]. Traditionally, porous materials have been either organic or inorganic materials. Perhaps the most common organic porous material is activated carbon. Porous carbon materials have various uses, including the separation and storage of gases, the purification of water, and solvent removal and recovery. In contrast, inorganic porous frameworks (e.g. zeolites) have been useful in separation and catalysis application [1]. One of the key advantages of MOFs comparing to organic/inorganic porous materials, is that their composition could be easily tuned by changing of the metal and/or the organic linker. Infinite range of linkers results in thousands of reported MOFs during past years with at least a few hundreds of them being porous to nitrogen gas [3].

MOFs are a class of crystalline materials with ultrahigh porosity (up to 90% free volume) and massive internal surface areas, extending beyond 6'000 m^2/g. MOFs are famous for their high surface areas, tunable pore size, and adaptable internal surface properties [4].

MOFs should be biologically and environmentally compatible for many applications. For instance, most biologically application, including drug delivery or intercellular imaging, requires non-toxic MOF materials. Moreover, bulk quantities of MOFs needed for many proposed applications. In order to decrease their environmental impact, bulk MOF materials should be either compatible or easily recyclable [2].
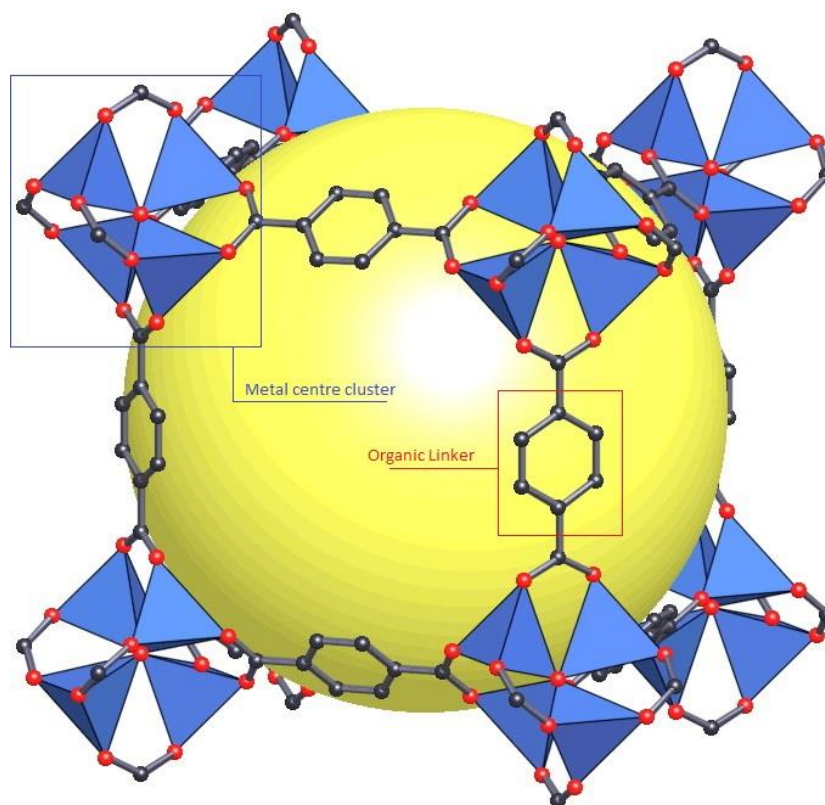
Figure 1.1-The MOF-5 structure shown as metal center cluster (ZnO$_4$ tetrahedra) joined by organic linker (benzene dicarboxylate) to give an extended 3-D cubic framework. Yellow sphere represents the largest sphere that can occupy the pores without coming within the van der Waals size of the framework [5].

1.1. MOF synthesis

Metal-organic frameworks can be synthesized in different methods. Different synthesis method of same reaction mixture, can lead to different MOFs. Methods can have a strong impact on reaction time, yields, or particle size and morphology. Thus, a detailed synthesis procedure is essential for obtaining the same structure. Different synthesis methods have been reported so far, some of them are room temperature synthesis, conventional electric heating, microwave heating, mechanochemistry , and ultrasonic. Here, we describe them briefly and in some cases a MOF synthesized with given method is reported.

Every chemical reaction needs some form of input energy. Normally metal-organic framework syntheses take place in a solvent and at temperature ranging from room temperature to approximately 250 ^{o}C. This energy may be provided by conventional electric heating, which can be an oven through

convection. Alternatively, referred energy can also be introduced by other means such as electric potential, mechanical waves (ultrasound), or mechanically.

1.1.1. Conventional electric heating method

This method is the most common route to synthesis metal-organic frameworks, which is carried out by conventional electric heating without any parallelization of reactions. One of the major parameters in this method is reaction temperature. Depending on the temperature range, this method cab be categorized into, solvothermal and nonsolvothermal. In 1985, Rabenau defined solvothermal as a reactions taking place in closed vessels under autogenous pressure above the boiling point of the solvent. Accordingly, nonsolvothermal reactions take place below or at the boiling point under ambient pressure[6].

To grow crystals from clear solution, the concentration of the reactants has to be adjusted in a way that the critical nucleation concentration is exceeded. This can typically accomplished by evaporation the solvent or by changing the temperature. The crystal growth occurs, as soon as particles exceeding the critical radius. Methods such as solvent evaporation of a solution of reactants, slow diffusion of reactants into each other lead to concentration gradients that allow the formation of MOFs. Concentration gradients can also achieved by applying a temperature gradient or slow cooling of the reaction mixture. Commonly, these methods lead to obtain large crystals which are suitable for structure determination[6].

Room temperature synthesis of some metal-organic frameworks is also reported. MOFs such as MOF-5, MOF-74, and ZIF-8 can be synthesized at normal room temperature (20-25°C) by mixing the starting materials. Some of these MOFs show good thermal and chemical stability. Generally, in solvothermal methods, several parameters such as solvent, pH, reaction time, and stoichiometry play a major role in the result of the synthesis.

1.1.2. Microwave heating method

Microwave synthesis method in based on the interaction of electromagnetic waves with mobile electric charges. These can be electrons/ ions in solid or polar solvent molecules/ ions in a solution. In solids, an electric current is formed and heating is due to electric resistance of the solid. In solutions, by applying suitable frequency, collision between the molecules happens and as a result the kinetic energy (temperature) of the system is increasing[6].

Commonly, this method of synthesis carried out at a temperature above 100 ^{o}C with usual reaction time of no more than 1 hour. Compare to conventional method, this method is faster but the produced crystals are usually smaller than conventional method. Several metal (III) carboxylate-based metal-organic frameworks have been prepared by this synthesis route[6].

The first reported microwave synthesized MOF was in 2005 by Jhung and co-workers. They have synthesized MIL-100 (Cr) using microwave irradiation. The reactant was heated at 220 ^{o}C in microwave for 4 hours and the X-ray diffraction patterns of resulting crystals showed a similar pattern for MIL-100 (Cr) synthesized at 220 ^{o}C for duration of 4 days which was the evidence of success[7].

1.1.3. Electrochemical method

This method was first reported in 2005 by researchers at a famous chemical company named "BASF". The main goal was the exclusion of undesired anions such as nitrate or chloride during syntheses. These anions may cause problem for the large-scale production processes. In this method, metal ions used instead of metal salts. The metal ions are continuously provided by anode to the reaction medium which contains a conducting salt and dissolved linker molecules. The metal formation on the cathode is avoided through using protic solvents[1], but as a result, H_2 is formed. The most interesting advantage of this method is the possibility of continuous process and the possibility to obtain higher solids content compared to normal batch reaction [6].

Researchers at BASF have studied this method with different combination of anode materials such as Zn, Cu, Co, and Mg and linker molecules such as 1,3,5-H_3BTC, H_2BDC, 1,2,3-H_3BTC and H_2BDC-$(OH)_2$[2]. They synthesized HKUST-1 (also known as MOF-199) with chemical formula of $Cu_3(BTC)_2(H2O)_3$ through this route. Synthesized material was compared with solvothermal synthesized of MOF-199, and the X-ray powder diffraction (XPRD) results showed the formation of referred MOF. However, electrochemically synthesized product exhibits low quality in thermogravimetric (TG) experiments and sorption experiments which is due to incorporation of linker molecules and/ or the conducting salt in the pores during crystallization[6].

---

[1] Solvent which contains unstable H^{+}
[2] BTC=1,3,5-benzentricarbozylate
BDC=1,4-benzenedicarboxylic acid
BDC-$(OH)_2$= 2,5-dihydroxybenzenedicarboxylate

1.1.4. Mechanochemical method

Mechanochemical synthesis (also known as solvent-free synthesis) is carried out through mechanical breaking of intramolecular bonds, which is followed by chemical transformation. This method of synthesis has multiple advantages, which makes it interesting. This method in carried out at room temperature under solvent-free conditions, which is environmentally friendly since no organic solvent is used. Other benefits of this route are, short reaction time (normally in the range of 10-60 min), and quantitative yields[6].

In 2006, Pichon et al. reported the first synthesized MOF through mechanochemical route. They synthesized a MOF with chemical formula of $Cu(INA)_2$[3] by grinding together copper acetate and isonicotinic acid for 10 minutes. The reaction had water and acetic acid as byproducts, these byproducts had been removed by heating at 200 ^{o}C for 3 hours. The resulting MOF was a microporous framework and had 3-dimensional connectivity[8].

The resulting framework was compared with solvothermal synthesized framework of $Cu(INA)_2.2H_2O$ and the XRPD patterns showed that the same structure had reached. However, there was an small difference between two patterns which was due to inclusion of acetic acid in the channels of mechanochemical framework instead of water molecules inside the structure of the solvothermal framework [8].

1.1.5. Sonochemical (ultrasound) method

This method relies on the application of high-energy ultrasound to reaction mixture. In liquids ultrasonic irradiation provides unique reaction conditions such as short reaction time, high temperatures, and high pressures which make it completely different from traditional sources of energy[9].

Ultrasound is cyclic mechanical vibration with a frequency range of 20 kHz to 10 MHz. Molecular dimensions are much lower than acoustic wavelengths. Hence, no chemical reaction takes place through direct interaction of ultrasound and molecules. Instead, a process called "acoustic cavitation"[4] is the reason of the chemical reaction. When liquids are irradiated with ultrasound, acoustic waves create bubbles and make the bubbles oscillate. These oscillating bubbles grow (tens of micrometers) meanwhile they accumulate the ultrasonic energy. Once the bubbles reach their maximum size, they

---

[3] INA=isonicotinic acid
[4] The formation, growth, and collapse of bubble in liquid

collapse. This collapse, releases the stored energy in the bubble with heating and cooling rate of $>10^{10}$ Ks^{-1}, temperatures of approximately 5000 K, and pressures of approximately 1000 bar[9].

1.2. MOF structure

Structure of metal-organic framework can be classified by their secondary building units (SBUs). SBU refers to the geometry of the units defined by the points of extension. However, the organic linker plays an important role in the topology of MOF, but SBUs dictate the final geometry of these materials. Figure 1.2 exhibits two secondary building units according to their inorganic units[5]. A complete review on the secondary building units according to their points of extension could be found in reference [10].
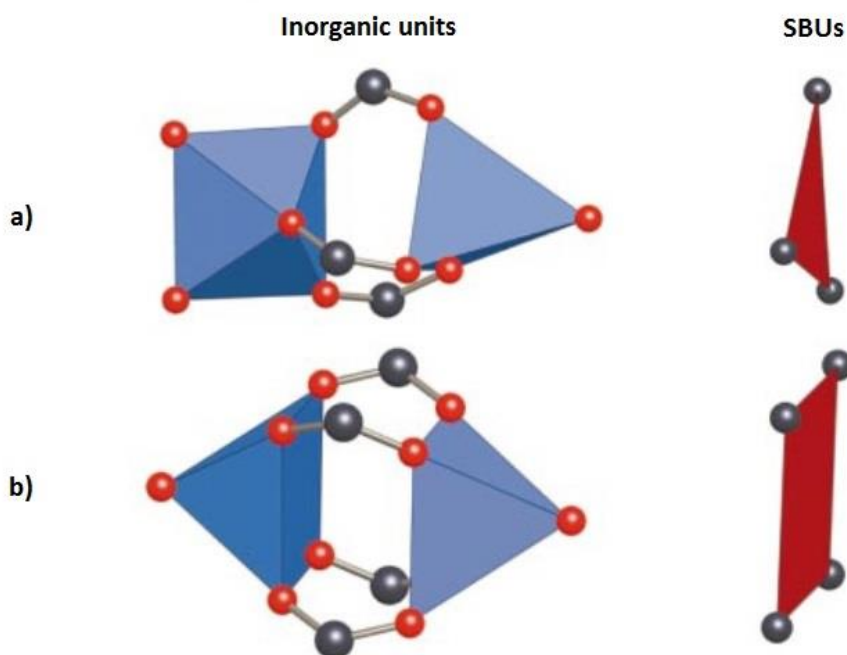
Figure 1.2- Examples of SBU from carboxylate MOFs. O, red; N, green; C, black. In organic units metal oxygen polyhedral are blue, and polygon defined by carboxylate carbon atoms (SBUs) are red. a) Triangle (three points of extension), b) Square paddle-wheel (four points of extension)[5].

In 2008, Collins and co-workers proven that the geometry of the SBU is dependent on the characteristics such as structure of the ligand, type of metal, metal to ligand ratio, solvent, and the source of anions to balance the charge of the metal ion[11].

MOFs are mostly porous; which means that they have void spaces within their structure. According to IUPAC pores are classified by their size range, which is micropores (<2 nm), mesopores (2-50 nm), and macropores (>50nm). Mesoporous and macroporous are attractive for catalysis applications because of

their large pores. Microporous materials can be good candidates for gas storage and separation due to the strong interactions between gas molecules and the pore walls[1].

Commonly the pores of MOFs are filled with the solvent molecules, which must be removed for most applications. One of the possible problems in removal of guest molecule is structural collapse. Generally, in large pores the possibility of collapse is higher.

1.3. MOF applications

Recently, metal-organic frameworks have received much attention owing to their wide range of applications. Being porous makes these materials interesting in areas such as hydrogen storage [12], gas adsorption and separation [13], catalyst [14], drug storage and delivery [1], and electrochemical [15].

1.3.1. Hydrogen storage

During past decades, researches focused to find suitable replacement for fossil fuels. An alternative fuel for automotive transportation with less carbon emissions become a first priority. Battery and fuel cell technologies are strong candidates to replace gasoline and diesel engines. In particular, hydrogen is an attractive energy carrier because it is carbon-free and abundantly available from water. Hydrogen must be compressed to very high pressures or stored cryogenically (at low temperature) [16].

Materials with large surface areas and low densities such as MOFs, porous carbons, zeolites and organic polymers, are attractive for hydrogen storage applications. Hydrogen storage capacity in these materials depends on their surface area and pore volume. The main limitation of MOFs usage in H_2 storage is the weak van der Waals interaction energy between H_2 and the surface of the material [12].

MOF-5[5] has been widely studied since, and turns out to be the best cryogenic storage material currently known. In 2003, the initial H_2 storage data were reported for MOF-5 (4.5 wt% at 77 K and 1 atm), although it was found later that the maximum H_2 uptake varies from 1.3 to 5.2 excess wt% at 77 K depending on the preparation and handling conditions. In 2010, Jeffrey R. Long et al. studied 6 references of MOF-5 preparation and handling conditions, and they suggested a new condition with better hydrogen uptake. They have minimized the exposure to water and air in their synthesis method, by which they have reached to one of the highest gravimetric capacity (7.1 excess wt% at 77 K and 40 bar) observed for a hydrogen storage material operating at 77 K [17]. Figure 1.3 shows the total and

---

[5] $Zn_4O(1,4\text{-benzene dicarboxylate})_3$

excess uptake of hydrogen for this material with referred synthesis conditions. In the same year (2010), Omar K. Farha et al. simulated a new metal-organic framework with a structure similar to MOF-5. The simulation results showed the highest excess H_2 storage capacity so far for MOFs with 99.5 mg/g at 56 bar and 77 K (NU-100) in Northwestern University. After reaching that high storage capacity through computational design, they synthesized the material successfully.
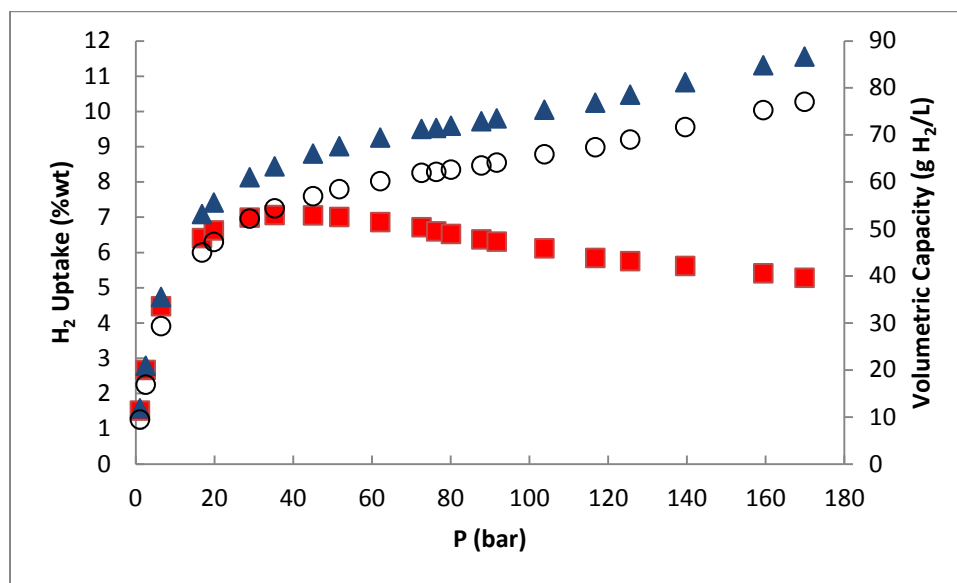
Figure 1.3- Hydrogen adsorption isotherms for MOF-5 prepared without exposure to air. Data were measured at 77 K by Jeffrey R. Long et al. and are shown as excess (filled red squares) and total (filled blue triangles) uptake. Open circles indicates the volumetric capacity of hydrogen (right-hand scale). Reprinted with permission from [17].Copyright 2007 American Chemical Society.

Excess uptake is the amount of gas taken up in addition to what would be present in the container with a volume equal to the pore volume within the sample. Total uptake is the amount of gas contained within the volume of the crystals, with includes both surface-absorbed molecules and pressurized gas within the pores [17].

1.3.2. Catalyst

As mentioned before, one of the key features of the MOFs is their porosity; this characteristic makes metal-organic interesting in catalyst area. Zeolites are the most commercially important classes of catalyst. MOFs have some of the catalytically relevant specifications of zeolites such as large internal surface areas and uniform pore and cavity sizes. First, comparing to zeolites, MOFs can be synthesized in much chemical variety because they also contain organic base. Second, stability (depends essentially on the cation coordination) of MOFs is lower than zeolites, which makes them weak catalysts for reactions

requiring forcing conditions. Third, persistence of microporosity after solvent evacuation is essential for gas-phase catalysis, but some MOFs collapse when solvent is removed (the larger the pore, the more likely the collapse). However, for catalysis of condensed-phase reactions this feature is not essential [14].

Pore system of the MOFs ranges from ultramicroporous to mesoporous, which gives them a remarkable opportunity for catalysis. The variety choice of structure, which facilitates pore-size tenability, is a great opportunity for designing MOFs with pore openings appropriate for generating size and shape selectivity. In addition to pore size, different pore topologies can be found for MOFs. For example, the pore structure can be one-dimensional (1-D) with straight channels, 2-D, or 3-D [18].

In 2009, David Farrusseng and co-workers reviewed the state of the art of catalytic MOFs, and they reported application of metal-organic frameworks in areas such as Lewis acid catalysis, Brønsted acid catalysis, base catalysis, C-C bond formation, polymerization, etc.

Omar K. Farha et al. studied metal-organic frameworks application as catalysts. They reported MOF usage in reactions catalyzed such as oxidation of olefin, oxidation of alkane, oxidation of sulfide, oxidation of polyphenol, oxidation of alcohol, reduction of nitroaromatic etc.[14] For example Y.Lu and co-workers examined the catalytic activity of [Co(BPB)].3DMF[6] for oxidation of cyclohexene by employing tert-butyl hydroperoxide as oxidant . They reported a fast and multiple turnover oxidation of cyclohexene in the presence of mentioned MOF, whereas no reaction occurs in the absence of catalyst under the same condition [19].

1.3.3. Gas adsorption and separation

Separation is a process that divides a mixture into its components, which is caused by a mass separating agent called adsorbent, or sorbent. Adsorptive gas separation includes passing a gas mixture through a columns packed with sorbent particles, or fixed-bed adsorbers to yield a product enriched in the more weakly adsorbed constituent. This is then followed by desorption of the strongly adsorbed component so that adsorbent can be reused. Separation is the opposite process of mixing and normally is not a spontaneous procedure. Selective adsorption leads to separation[20].

---

[6] Cobalt (II) 1,2-bis(4'-pyrazolyl)benzene in dimethylformamide.

Adsorptive gas separation processes can be divided into two types: bulk separation (adsorption of a significant fraction, 10% by weight or more from a gas stream) and purification (less than 10%[7] by weight of a gas stream is adsorbed)[20]. High separation power can be reached by continuous contact and equilibration between the gas and adsorbent, for this purpose cyclic process such as thermal swing adsorption (TSA) cycles, pressure swing adsorption (PSA) cycles are available[21].

Every component has its own adsorption capacity as an adsorbent. The difference between adsorption capacities is the foundation of gas separation in adsorptive separation. The performance of any adsorptive separation or purification process is directly determined by the characteristics of the adsorbents in both adsorption equilibrium and kinetics. In addition to suitable mechanical properties, a promising adsorbent should have favorable adsorption kinetics and regenerability as well as good adsorption capacity and selectivity. To satisfy these requirements, the adsorbent should possess not only reasonably high surface area, but also relatively large pore sizes for porous materials to allow adsorbate molecules to approach the interior surface[21].

There are four major mechanisms for gas adsorptive separation by a porous material which can be reached by one or several of these mechanisms[22][20]:

(1) *Molecular sieving effect*; gas mixture components are either allowed or prevented from entering to the pores of an adsorbent, because of size and/or shape exclusion. The allowed components are subsequently adsorbed while the prevented components don't adsorb.

(2) *Thermodynamic equilibrium effect*; because of different adsorbate surface and/or adsorbate packing interaction, preferential adsorption of certain components over others occurs on the surface of and adsorbent.

(3) *Kinetic effect*; because of different diffusing rates, certain components enter the pores and become adsorbed faster than other components.

(4) *Quantum sieving effect*; because of quantum effect, some light molecules have different diffusing rates in narrow micropores, which allows such molecules to be separated.

---

[7] Usually <2%
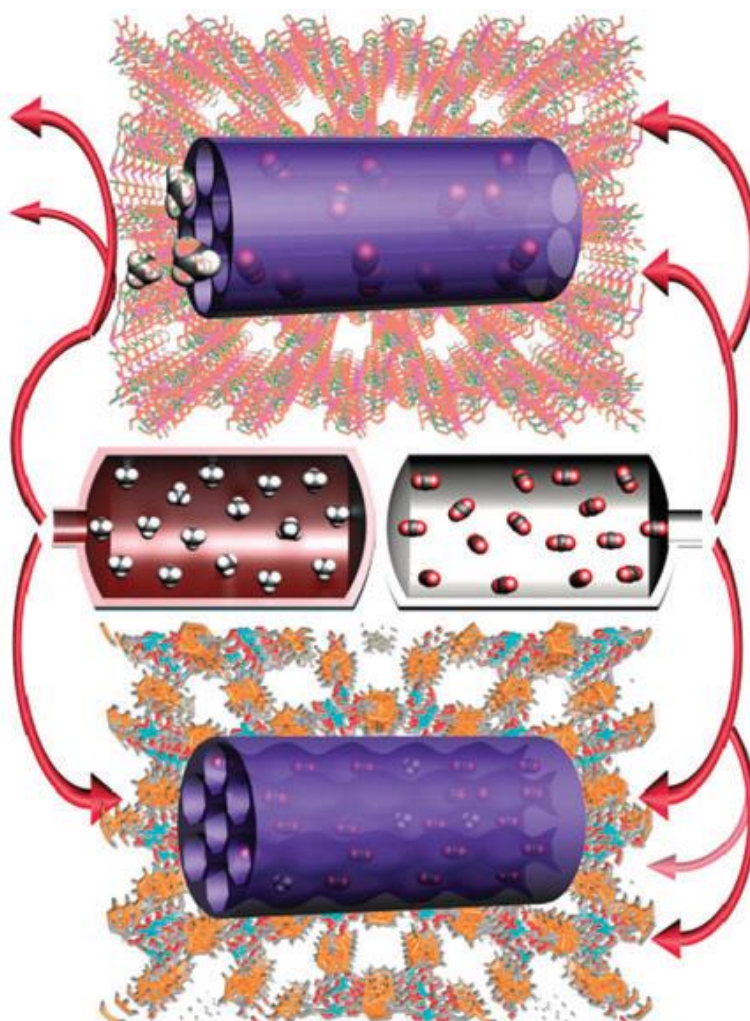
Figure 1.4- Schematic illustration of selective gas adsorption in rigid MOFs (top: the molecular sieving effect, bottom: thermodynamic equilibrium effect)[21].

MOFs can be categorized into flexible and rigid. Flexible MOFs have dynamic, "soft" frameworks which are sensitive to external stimuli, such as temperature, guest molecules, and pressure, while rigid MOFs have relatively stable and robust porous frameworks with permanent porosity[23]. Metal-organic frameworks features such as large surface area, adjustable pore size and thermal stability, gives them a decent opportunity to be used as adsorbents for gas separation. Research on MOFs is in the early stage, and a few numbers of them have been tested for their adsorption properties. The adsorption selectivity in rigid MOFs may be related to the molecular sieving effect and/ or preferential adsorption based on the different strengths of adsorbent-adsorbate and adsorbate-adsorbate interaction. Figure 1.4, presents a schematic illustration of selective gas adsorption in rigid MOFs[21].

Adsorption behavior of MIL-53 with chemical formula of $Cr(OH)(BDC)$, which is a flexible MOF, has been studied by Bourrelly and co-workers. As synthesized MIL-53 has a molecule of water inside its structure, dehydration of this material can occur by heating it at temperature of 100 ^{o}C. Dehydrated MIL-53 shows a typical CH_4 adsorption behavior for a microporous material, while the adsorption of CO_2 reveals two steps (Figure 1.5). The adsorption of CO_2 is higher than CH_4, which is expected because CO_2 has a significant quadrupole moment, whereas CH_4 is nonpolar[24].
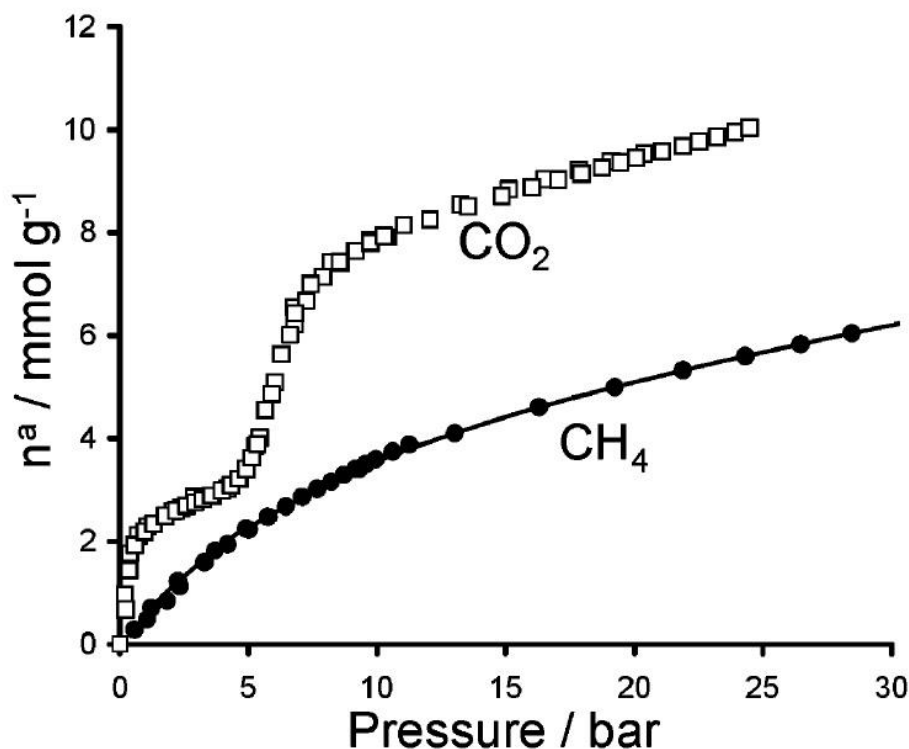
Figure 1.5- CO_2 and CH_4 adsorption isotherm of dehydrated MIL-53 at 304 K. Reprinted with permission from [24].Copyright 2005 American Chemical Society.

In 2008, Youn-Sang Bae et al. synthesized a MOF with formula of Zn_2 $(NDC)_2(DPNI)$[8] by two different routes: first at 80°C for two days with conventional heating, and second at 120°C for 1 hour using microwave heating. They reported a selectivity of 30 for CO_2 over CH_4 for the microwave sample, which is among the highest selectivities reported for this separation[25].

---

[8] NDC=2,6-naphthalendicarboxylate
DPNI=N,N'-di-(4-pyridyl)-1,4,5,8-naphthalene tetracarboxydimiimide

1.3.4. Electrochemical

The electrochemical application of MOFs is quite a new investigation on this type of materials. Metal-organic frameworks may be used for energy storage and conversion. For instance, MOFs can be used for supercapacitors, rechargeable batteries and fuel cell. Electrochemistry, is the study of chemical reactions, include electron transfer, at the interface of electrode and electrolyte. A chemical reaction that involves electron transfer between molecules is called oxidation/reduction or "Redox" reaction. Metal cations are redox source inside the structure of metal-organic frameworks; these cations can provide a pathway for electrons. In addition, decent selecting of organic linker may improve the charge transfer inside the framework[15].

Two applications of MOFs in electrochemical area are briefly reported in this work; Li-ion battery and Proton Exchange Membrane (PEM) fuel cell.

Li-ion battery:

One of the most common rechargeable batteries is lithium-ion (Li-ion) battery and it is widely used for portable electronics. Lithium intercalated/alloyed in the anode and during discharge; Li is oxidized to lithium cation (Li^+) and transfers to the cathode.

Three attempts have made to apply MOFs for positive electrode in Li-ion batteries and only one of them was successful. Zinc and Nickel based MOFs was used to achieve this goal, using of Ni-based microporous phosphate led to transformation of the solid into a nanocomposite electrode made of Ni nanoparticles and Li_2O matrix. The other attempt with Zn-based MOF is also came up with the similar result to nickel based, in the presence of Li ions Zn-based framework decomposed into a zinc based nanocomposite matrix containing Li_2O.

In contrast, Ferey et al. realized that stronger metal-oxygen bonds my lead to suitable stability; therefore, they used metals such as Cr^{3+} and Fe^{3+} with higher oxidation state than Zn or Ni. The suitable metal-organic framework was founded to be MIL-53 (Fe). H_2O, 15 % wt carbon was added to this material to be used in the positive electrode, while the negative electrode was Li-metal. $Li_{0.6}Fe(OH)_{0.8}F_{0.2}(BDC).H_2O$ showed a maximum uptake of lithium upon discharge while it was fully reversible for at least 50 cycles [26][15].

PEM fuel cell:

The need to switch from internal combustion engines to a low emission engines was gained much attention during past decades, fuel cells are one of the main leader for this replacement. Fuel cells can be characterized by the electrolyte of them. Every fuel cell is consisting of three parts; *Anode* where fuel is oxidized into electrons and protons, *Cathode* where oxygen is reduced to oxide species, and *Electrolyte* where oxide ion or protons (depending on the type of electrolyte) are combined with oxide or protons to produce electricity power and water.
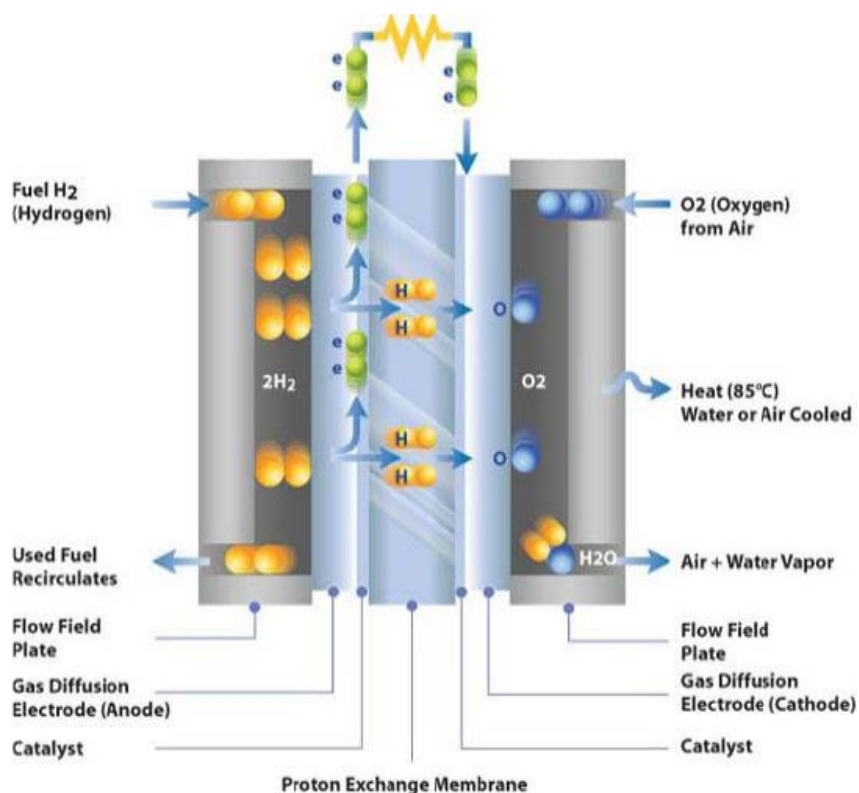
Figure 1.6-Schematic representation of a PEM fuel cell consisting of catalyst layers, gas diffusion electrodes and proton exchange membrane.

PEM fuel cell is among the low temperature operating (50-100 ^{o}C) fuel cell, its electrolyte is a solid polymer (such as Nafion). The heart of a PEM fuel cell is its membrane electrode assembly (MEA) with a thickness of less than a few hundred microns. Liquid water should be present in the membrane for effective proton conducting, and this is why PEM fuel cells should operate in low temperatures. MEA performance depends on its electrocatalyst technology. The catalysts form thin gas-porous electrode layers on either side of the membrane[27].

Today, the most famous and applicable catalyst used in MEA is platinum-based materials. One of the key sources of voltage loss in H_2/air fuel cells is the slow kinetics of the Oxygen Reduction Reaction (ORR); even in the best Pt-based catalyst, this problem faced. Finding an alternative for platinum-based catalyst is one of the major research areas since platinum is expensive and its availability is low. Suitable and low cost alternative catalysts for ORR may lead to decrease the overall cost of PEM fuel cells.

MOFs have some features such as available metal cations in their structure, high micropore surface area and high volumetric density of metal-ion sites, which make them suitable to be pyrolyzed, in order to synthesize non-precious metal catalysts for ORR[15].
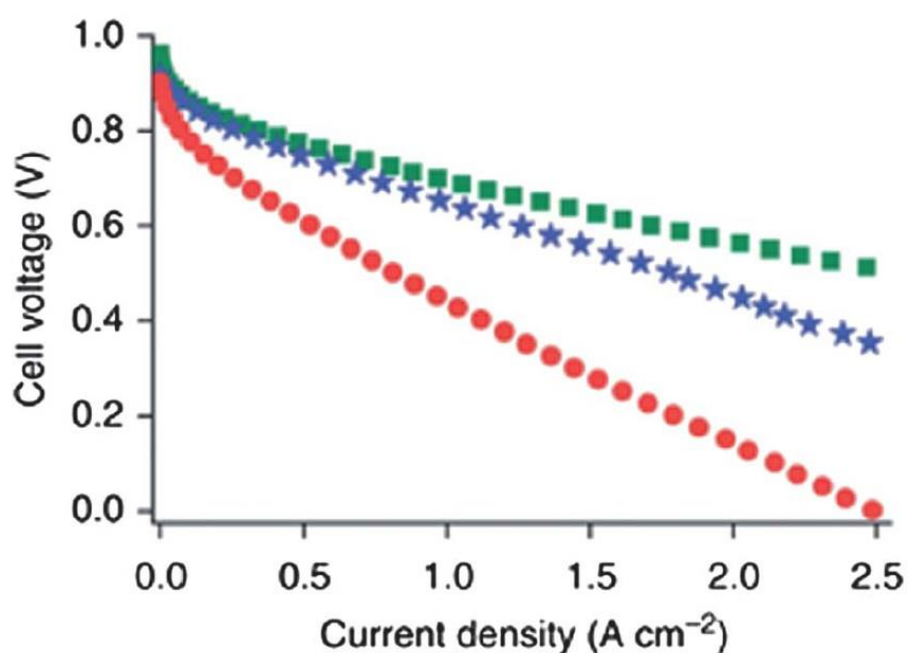
Figure 1.7- Polarization curves for PEM fuel cell of H_2/O_2. State-of-the-art Pt-based cathode (0.3 mg_{Pt} cm^{-2}, green squares), Fe-based cathode catalyst synthesized using ZIF-8 (blue stars) and Fe-based cathode catalyst synthesized using high surface area carbon black instead of ZIF-8 (red circles). Preprinted by permission from Macmillan Publishers Ltd: Nature Communications [28], copyright 2011.

In 2011, Proietti and co-workers produced ORR-catalyst precursor by mixing zinc based ZIF-8 (Zn^{II} zeolitic-imidazolate-framework) with ferrous acetate and 1,10-phenanthroline. ZIF-8 used for that study had chemical formula of $Zn(MeIm)_2$ [9] and its structure exhibits a nanopore topology resulting from bridging the Zn(II) centers to nitrogen atoms of imidazolate ligands. A cathode with best electrocatalyst

---

[9] MeIm=2-methylimidazolate

was prepared by pyrolysis at 1050 ^{o}C in argon, then 950 ^{o}C in ammonia. After pyrolysis, the catalyst precursor transformed into a nitrogenated microporous carbon structure hosting FeN_x active sites. This new catalyst has been tested in H_2/O_2 proton exchange membrane fuel cell and it had a current density of 1.2-1.3 A cm^{-2} at 0.6 V, which is among the best reported performance for non-precious metal catalyst yet reported[28] [15]. Figure 1.7 compares the polarization curve of platinum-based cathode, cathode catalyst synthesized in this work, and ferrous –based cathode catalyst synthesized with carbon black instead of ZIF-8.

New results from above MOF derived catalyst brought hope that may be the search for the suitable substitute for platinum based can go to next step with the development of non-precious metal catalyst. Meanwhile, the stability of these catalysts could be the next concern of this research area.

1.3.5. Drug storage and delivery

Traditionally, there were two routes for controlled release of drugs, "organic route" and "inorganic route". In organic route, either biocompatible dendritic macromolecules or polymers are used, which can be applied to encapsulate a wide range of drugs. However, there are some difficulties to accomplish a controlled release when there is no well-defined porosity. In contrast, inorganic route is a method in which inorganic porous solids or mesoporous silicate materials are the hosts of the drug. The limitation of this method is its low drug-loading capacity[29].

MOFs can present a third route in this fashion; the "hybrid route" which can have a high porosity with the presence of organic groups in the framework may lead to accomplish both high drug loading and controlled release. Ferey et al. selected MIL-100 and MIL-101 mostly because of their pore size and they studied these materials for the adsorption and delivery of Ibuprofen[29].

MIL-100 and MIL-101 are initially hydrated, their crystallinity remain unchanged after water evacuation. Dehydrated form of these MOFs was used to adsorb Ibuprofen. X-ray powder diffraction of materials after drug loading showed that their structures are retained after the adsorption. Moreover, the adsorption of N_2 was tested to check the possible space for more adsorption. Nitrogen adsorption results showed that there was approximately no adsorption, which was the evidence of complete adsorption of Ibuprofen in the pores leaving no space for nitrogen to enter the pores. Figure 1.8 displays the kinetics of Ibuprofen delivery to simulated body fluid at 37 ^{o}C with continuous stirring[29].
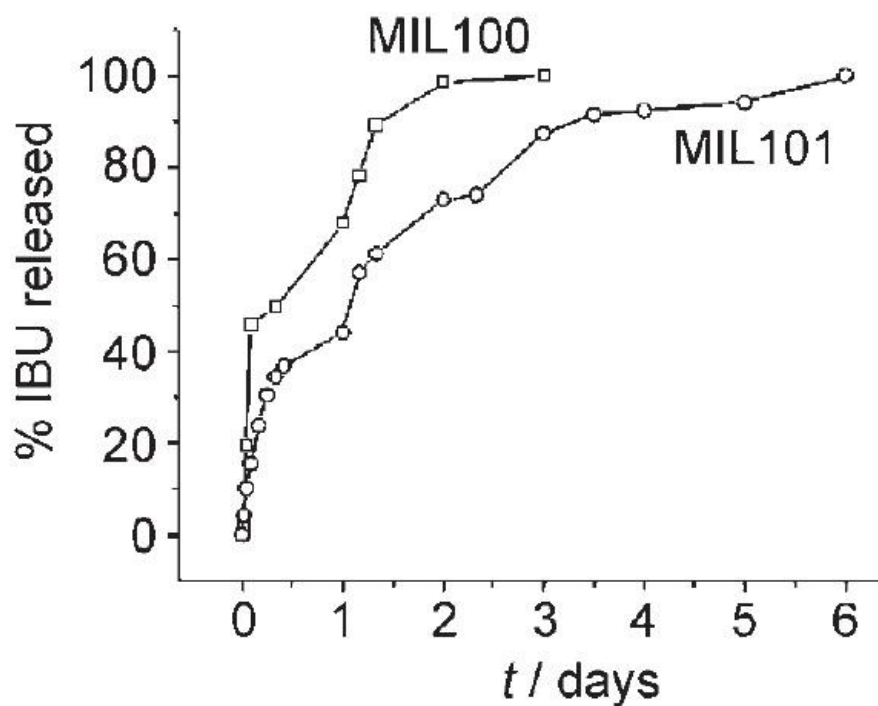
Figure 1.8- Ibuprofen delivery for MIL-100 and MIL-101. Reprinted with permission from [29], Copyright 2006 Wiley-VCH Verlag GmbH & Co. KGaA, Weinheim.

MIL-100 has been widely studied for its potential of drug storage. In 2012, Horcajada and co-workers reviewed metal-organic frameworks in biomedicine and they reported using this MOF for delivery of drugs such as busulfan, cidofovir, doxorubicin and so forth[3].

One of the most important aspects of MOF application in this area is their toxicity. However, there are wide ranges of toxicologically acceptable MOFs, which can be used in healthcare. The entire metal-organic framework composition should be tested for its toxicological behavior; because it may, has various toxic molecules (ligands or solvents) in its structure. Moreover, the performance of drug release can be highly affected by stability and biodegradability of MOFs since there is an extreme change of pH and composition in body fluid. For instance, MOF-5 is completely unstable in the presence of water however some other MOFs such as ZIF-8 and MIL-100 have been proven to be hydrothermally stable[3].

In 2008, Rieter et al. reported a platinum-based nanoscale coordination polymer (NCP). Pt-based drugs are used as the frontline treatment for a number of cancers. NCP-1 with formula of $Tb_2(DSCP)_3(H_2O)_{12}$, was structurally amorphous, showing no peaks in XRPD analysis. NCP-1 was soluble in water therefore; they encapsulated the material in shells of amorphous silica in order to protect it from rapid dissolution in water. The resulting silica coated material, NCP-1', was in turn divided to two different materials

depending on the reaction time and amount of TEOS[10] used. NCP-1'-a, was resulting from 2 hours of TEOS treatment which yielded a shell thickness of 2 nm. NCP-1'-b, was obtained after 4 hours of TEOS treatment, which had a silica shell thickness of 7 nm. Figure 1.9 shows the release behavior of dialyzed samples against HEPES[11] buffer (pH=7.4) at 37 $^{\circ}$C. These release rates are sufficient for drug to circulate in the body and accumulate in tumor tissue[30].
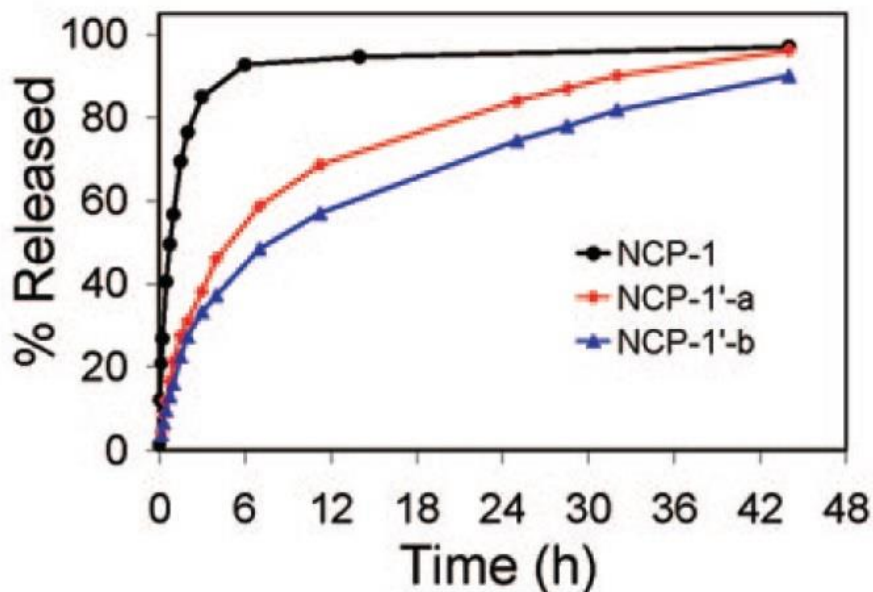
Figure 1.9- Pt% released profile for NCP-1, NCP-1'-a, and NCP-1'-b. Reprinted with permission from [30], Copyright 2008 American Chemical Society.

In order to improve the cellular uptake of NCP-1' *in vitro*, silyl-derived cyclo (RGDfK)[12] was grafted to the surface of silica coated material. Cyclo (RGDfK) is a small cyclic peptide, which shows high binding affinity for the $\alpha_V\beta_3$ integrin, a protein overexpressed in cancer cells. They reported IC$_{50}$ (50% Inhibitory Concentration) value of 9.7 and 11.9 [Pt] μM for cyclo (RGDfK)-targeted NCP-1'-a and NCP-1'-b, respectively[30].

---

[10] TEOS= Tetraethyl orthosilicate
[11] HEPES= 4-(2-hydroxyethyl)-1-piperazineethanesulfonic acid
[12] Cyclo (RGDfK)= Cyclo (Arg-Gly-Asp-D-Phe-Lys)= $C_{27}H_{41}N9O_7$

Metal-organic framework   18

1.4. MBioF

Metal-biomolecule frameworks (MBioFs) are MOFs with biomolecules (such as amino acids, peptides, nucleotides, etc.) as an organic linker. These types of frameworks can exhibit several advantages; some of these benefits are as follow[2];

- Simple biomolecules are naturally accessible (examples sugars, amino acids, etc.) therefore, low-cost large-scale production of these frameworks is possible.
- Comparing to MOFs, MBioFs are biologically compatible.
- Biomolecules are structurally rigid or flexible. Therefore, the resulting MBioF can be either rigid or flexible.
- Biomolecules can have many different metal-binding sites, which give them the opportunity of having various coordination modes and as a result, countless MBioF structures.
- Finally, several biomolecules are chiral. Consequently, the resulting MBioF can be chiral, which are suitable for applications such as separation and catalysis.

α-Amino acids (AAs) have a general formula of NH_2CHRCO_2H (where NH_2 is the amino group, CO_2H is the carboxylic acid group, and R is the organic side chain). Peptides and proteins are formed by linking AAs together through amide bonds. Proteins and peptides are excellent organic ligands and metals can be coordinates through their amino and carboxylate group.

MBioFs with AAs as organic linker can be categorized to three major types depending of their metal ion bridges. They are either constructed from (a) natural AAs ligand and metal ions; (b) metal ions, natural AAs, and additional bridging anions and polydentate organic ligands; or (c) metal ions and chemically-modified natural AAs (example AAs modified with additional metal-binding group)[2].

A complete study of MBioFs can be found in reference [2] and [3]. However, a detailed study of peptide-based MBioFs is presented in chapter 2 of this work.

1.5.   Objective of the study

The objective was to assemble GlyAsp-based MBioFs. The first objective was to obtain crystalline materials suitable for further analyses. The crystalline materials (two different frameworks) were characterized by X-ray diffraction, scanning electron microscopy, thermogravimetric analysis, and CO_2 equilibrium adsorption isotherm.

Peptide-based metal frameworks are showing interesting applications in areas such as (i) biomedicine and (ii) chemical engineering.

(i)   This work is a part of longstanding project to prepare ArgGlyAsp-based framework, it is well known that ArgGlyAsp (RGD) tripeptide targets $\alpha_V\beta_3$ integrin, protein overexpressed in many tumors. Therefore, RGD-based MBioF would have a potential to be used in applications such as imaging/early detection of tumor cells and delivering of antitumor agents. Notwithstanding, oligopeptides are very flexible and it is difficult to assemble them in crystalline frameworks. Thus, it is advisable to start by a shorter linker (GlyAsp) instead of the full tripeptide (ArgGlyAsp).

(ii)   On the other hand, dipeptide-metal frameworks revealed very interesting properties as gas adsorbents. Zinc-dipeptide compounds (Rabone et al. 2010) display a framework with a so-called ''breathing'' behavior, contracting and expanding according to the molecular size of the adsorbed species, mimicking the behavior of certain protein membrane channels. In some cases, i.e. $[Zn(GlyThr)_2]$, they also display an interesting CO_2/CH_4 sorption selectivity.
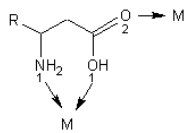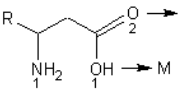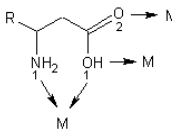
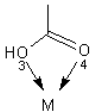# Chapter 2

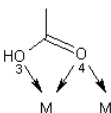## 2.   Peptide-based MBioFs
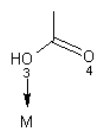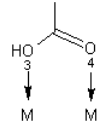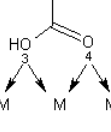
2.1.   Introduction

As mentioned earlier in chapter 1, MBioFs are metal-organic frameworks with at least one biomolecule as organic linker. The term peptide-based MBioF is referred to a metal-organic framework which has peptide molecule as an organic linker. A well understanding of some basic terms and definition is essential for studying these frameworks.

- **Metal complex:** a compound formed from a Lewis acid and a Brønsted base.
- **Ligand:** The Brønsted bases attached to the metal ion in metal complex.
- **Coordination number:** The number of electron pairs arising from the ligand donor atoms to which the metal is directly bonded.
- **(mono-) (bi-) (poly-) dentate:** A ligand can bond to a metal ion through donor atoms, in different modes. These modes can be categorized to monodentate (single donor atom), bidentate (two donor atoms), and polydentate (several donor atoms).
- **Chelate complex:** When a bi- or polydentate ligand uses two or more donor atoms to bind to a single metal ion, a chelate complex forms.
- **μ_i:** The character μ used to denote an atom or group which bridges to metal centers. The number of bridged atoms indicated with i subscript.

Amino acids are tending to form metal complex, they can coordinate metal ions via bi- or tridentate (three donor atoms) bridging modes. Metal ions may link to C-terminus and/or N-terminus of α-carboxylate group of the AAs or the side chain of them. When this occurs, extended metal ion-AA framework can be created. To date, most of reported pure AAs-based coordinated networks, had 1-D structure. However, there are some examples with 2-D and 3-D extended structures[2]. For instance, Fleck and co-workers reported a 2-D metal ion-AA framework of Gly with Ni(II) metal ions in a 2:1 fashion. In the reporting network, each octahedral Ni ion was linked to another four metal ions through four Gly ligands thus, adopting a μ_2-O_1:O_2 coordination mode[31]. Table 2.1 illustrates some potential coordination modes for amino acids.

Table 2.1- Selected potential coordination modes for metal ion in amino acids.

Structure	Coordination mode	Main AAs chain/side chain
	bidentate (μ_2-N_1O_1:O_2)	main chain
	bidentate (μ_2-O_1:O_2)	main chain
	tridentate (μ_3-N_1O_1:O_1:O_2)	main chain
	monodentate (μ_1-O_3O_4)	side chain
	bidentate (μ_2-O_3O_4:O_4)	side chain
	monodentate (μ_1-O_3)	side chain
	bidentate (μ_2-O_3:O_4)	side chain
	tridentate (μ_3-O_3:O_3O_4:O_4)	side chain

2.2. Dipeptide-based MBioFs

Dipeptides are composed of two amino acids linked by peptide bond. Peptide bond in a chemical bond formed between two molecules when the carboxyl group of one molecule links to the amino group of the other molecule, which follows by release of water (reaction 2.1).

Reaction 2.1
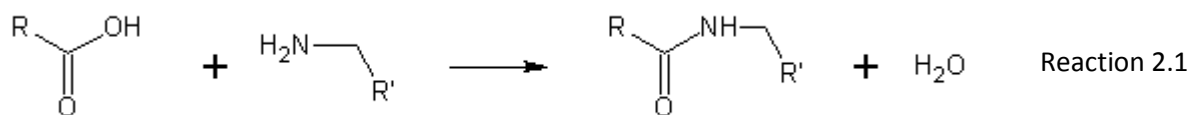
Both carboxyl group and amino group of a peptide can coordinate metal ions via different coordination modes. The amino group usually coordinates to metal ions in a monodentate or chelating fashion(figure 2.1) [2].

The first dipeptide-based MBioF was reported in 1996 by Takayama et al. They used GlyGly dipeptide with Zn(II) and Cd(II) metal salts. These authors synthesized three MBioFs by adjusting the pH to 6 and 9. At pH 6, they obtained 2-D frameworks with formula of $[M(GlyGly)_2].2H_2O$ (where M is Zn(II) or Cd(II)). Each octahedral metal ions of zinc or cadmium was linked to four other metal ions through GlyGly ligands. Each GlyGly ligand bridges two metal ions; a five-membered chelate ring was formed between the terminal amino group and the adjacent O, and a monodentate mode through the terminal carboxylate group. At pH 9, only Cd(II) framework formed, a novel 2-D MBioF formulated as $[Cd(GlyGly)_2].H_2O$, which each octahedral cadmium ions was bridged to six other Cd(II) ions by four GlyGly ligands. The terminal carboxylate group links to two metal ions, and amino group bridges to another Cd(II) ion in a monodentate mode[32].
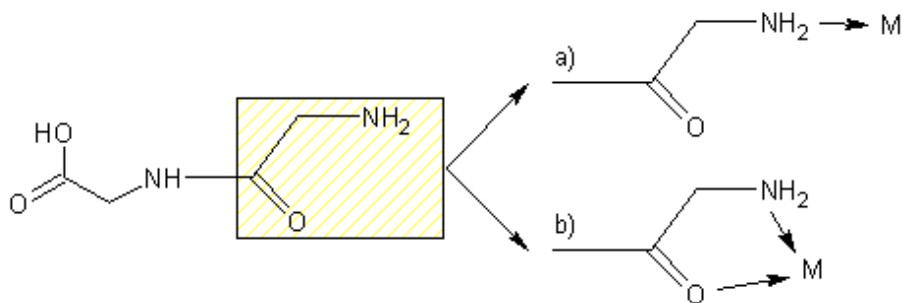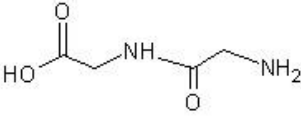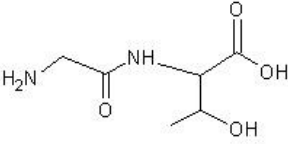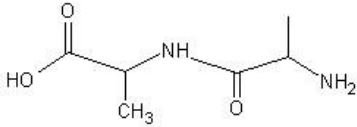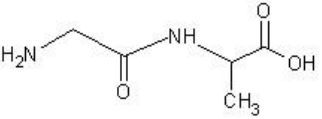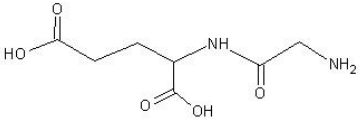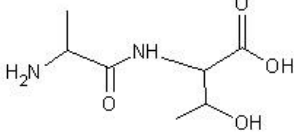
Figure 2.1- Presentation of potential coordination modes for the amino group of GlyGly dipeptide; a) monodentate mode, b) five-membered chelate ring.

To date, small number of dipeptide-based MBioFs has been reported. Some of these frameworks are summarized in table 2.2. Here, in this work three of these frameworks ([Cd(AlaThr)$_2$].4H$_2$O, [Zn(GlyAla)$_2$].(solvent), and [Zn(GlyThr)$_2$].CH$_3$OH) were selected to discus in more details.

Table 2.2- A summary of dipeptide-based metal-biomolecule frameworks.

Dipeptide	Metal ion(s)	MBioF(s) formula	Ref.
GlyGly	Cd(II), Zn(II)	[Cd(GlyGly)$_2$].2H$_2$O, [Zn(GlyGly)$_2$].2H$_2$O, [Cd(GlyGly)$_2$].H$_2$O	[32]
GlyThr	Zn(II)	[Zn(GlyThr)$_2$].CH$_3$OH	[33]
AlaAla	Cd(II)	[Cd(AlaAla)]	[34]
GlyAla	Zn(II)	[Zn(GlyAla)$_2$].(solvent)	[35]
GlyGlu	Pb(II), Cd(II)	[Pb(GlyGlu)(H2O)$_{1/2}$].ClO$_4$, [Cd(GlyGlu)$_2$].3H$_2$O	[36]
AlaThr	Cd(II)	[Cd(AlaThr)$_2$].4H$_2$O	[34]

[Cd(AlaThr)$_2$].4H$_2$O[34]**:**

This framework was synthesized at room temperature using base diffusion method with ultrasound assistant. A solution of 0.06 mmol of CdAc$_2$ and 0.12 mmol of AlaThr in 2 mL of water was sonicated for 5 min with gentle shaking at 150 w using ultrasonic bath. This solution was placed in a 5 mL glass vial, which was in turn was placed in a 20 mL screw-capped vial. Two milliliters of 2% triethylamine solution was added to the 20 mL vial and sealed with cap. Needle crystals with 60% yield (based on cadmium) were grown after about 3 weeks.

The crystal of this framework was monoclinic with space group of *C*2. Its structure exhibited a 2-D topology in which four peptides were linked together by four cadmium ions (figure 2.2). As shown in figure 2.2a each octahedral Cd(II) ions are linked to another four metal ions through four peptide ligands; two of which through the C-terminus carboxylate group (monodentate), and the remaining four via two different chelate rings through the N-terminus (NH$_2$- and amide carbonyl).
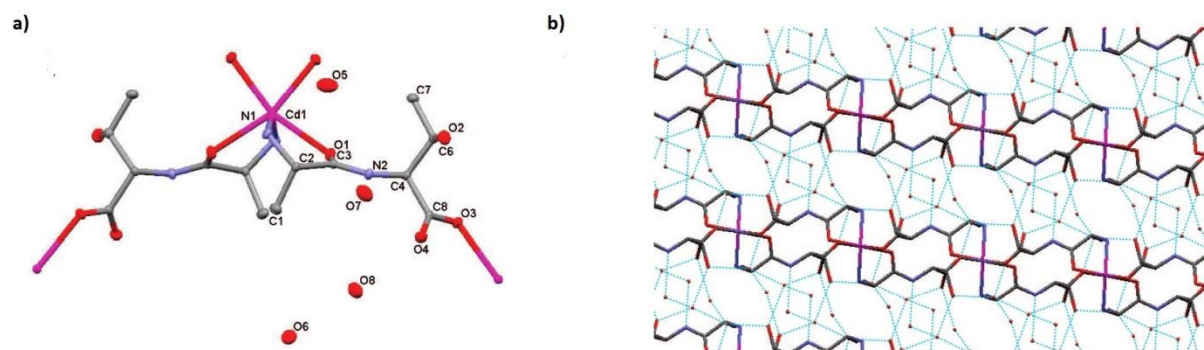
Figure 2.2- (a) Structure of [Cd(AlaThr)2].4H2O. **(b)** View along the crystallographic b axis (blue networks shows the hydrogen bonds).Reprinted with permission from [34], Copyright 2008 American Chemical Society.

[Zn(GlyAla)$_2$].(solvent)[35]**:**

Solvothermal method is used to synthesize this framework. A solution of 0.5 mmol of GlyAla and 0.25 mmol of zinc nitrate hexahydrate in a mixture of 90% methanol and 10% 1M aqueous NaOH, was heated to 85 ^{o}C for 1 hour with heating rate of 2 ^{o}C.min^{-1} and cooling rate of 0.2 ^{o}C.min^{-1}, resulting crystalline product with 75% yield.

The crystal of this framework was orthorhombic belonging to the space group P2$_1$2$_1$2. A 2-D structure was formed which, had a 1-D square-shaped pore along the *c* axis (figure 2.3b). In which, each

tetrahedral zinc ions were linked to four other metal ions through four peptide ligands; two dipeptide ligands were coordinated by the C-terminal Ala carboxylate groups (in monodentate mode) and the other two via N-terminal Gly amine groups (in monodentate mode) (figure 2.3a).
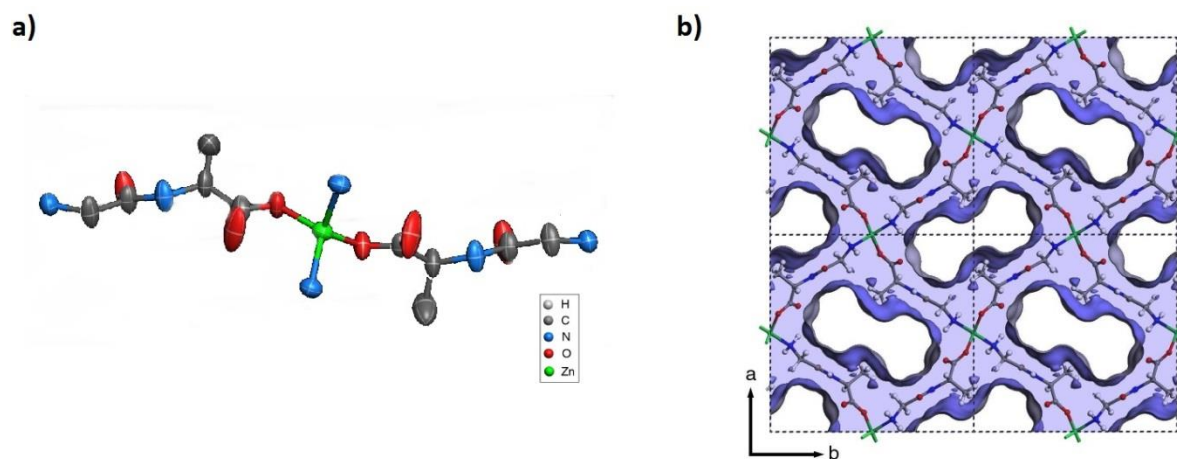
Figure 2.3- (a) Structure of [Zn(GlyAla)$_2$] above 298 K. **(b)** Representation of 1-D pore along the c axis at 298K (after solvent evacuation). Reprinted with permission from supporting online material of [35], Copyright 2010, American Association for Advancement of Science.

The solvent within the structure of this framework can be removed reversibly to obtain desolvated framework. According to thermogravimetric analysis (TGA) of the [Zn(GlyAla)$_2$]. (solvent), the first weight loss (15.4%) occurs in the temperature range of 35-250 ^{o}C which, corresponds to solvent loss. The next weight loss (64.5%) occurs in temperature range of 250-700 ^{o}C which, agrees with decomposition of [Zn(GlyAla)$_2$] to ZnO (figure 2.4a).

This framework shows a phenomenon called "breathing". Breathing phenomenon consists of two successive crystal-to-crystal transformations during adsorption process. In which, the pore volume of flexible framework is changing from large pore state to narrow pore state, and back again to the large pore structure[37].

Breathing phenomenon reduced the pore volume of the desolvated framework during CO_2 adsorption by changing the φ torsion angle of the methyl group of the Ala. The CO_2 adsorption isotherm of desolvated framework at 273 K indicates two steps, first at pressure range of 0-2 bar showing an small adsorption (non-porous structure), and second at pressure range of 2-15 exhibiting higher mass uptake (porous structure) (figure 2.4b).
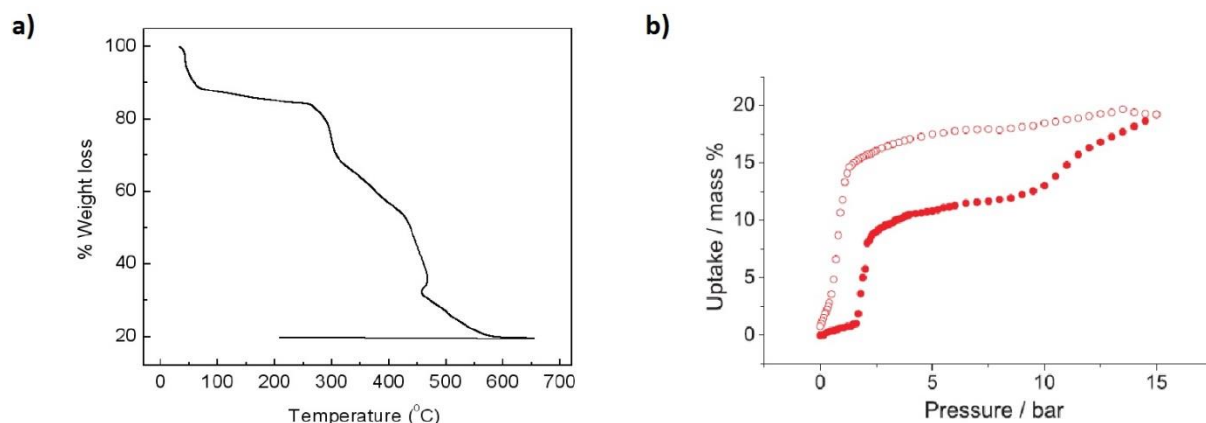
Figure 2.4- (a) Thermogravimetric analysis of [Zn(GlyAla)$_2$].(solvent) **(b)** CO$_2$ sorption isotherms of [Zn(GlyAla)$_2$] at 273 K (closed and open symbols represent adsorption and desorption, respectively). Reprinted with permission from [35], Copyright 2010, American Association for Advancement of Science.

[Zn(GlyThr)$_2$].CH$_3$OH[33]**:**

This framework was synthesized by the same group who produced the [Zn(GlyAla)$_2$].(solvent). The synthesis (solvothermal method) procedure is similar to that MBioF with small change in the solvent. A solution of 0.05 mmol of zinc nitrate hexahydrate and 0.1 mmol of GlyThr in methanol and 0.08 mmol of NaOH (aq) 1M, was heated to 85°C with heating rate of 2 $^{\circ}$C.min^{-1} and cooling rate of 0.5 $^{\circ}$C.min^{-1}, resulting in colorless crystals with yield of 70%.
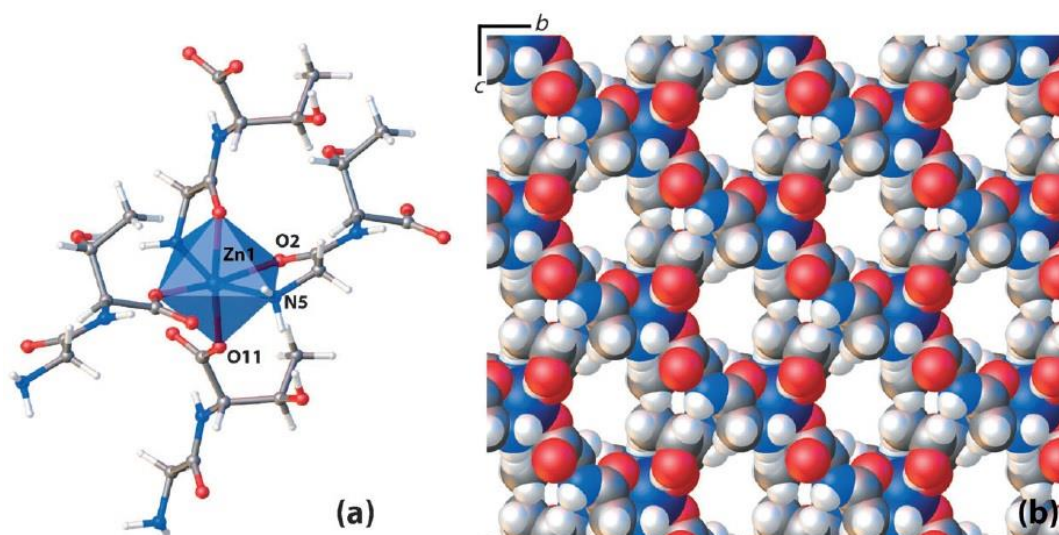
Figure 2.5- (a) Octahedral coordination of the peptide around Zn(II) ion of [Zn(GlyThr)$_2$].MeOH. **(b)** Space-filling representation of [Zn(GlyThr)$_2$], showing the 1-D pores along the a axis. Reprinted with permission from[33], Copyright 2012 Wiley-VCH Verlag GmbH & Co. KGaA, Weinheim.

The crystalline material of this framework had monoclinic structure belonging to *I*2 space group. The framework exhibits 2-D structure with 1-D pores along *a* axis (figure 2.5b). Each octacoordinated Zn(II) ions are linked to four dipeptides; two peptides ligands are coordinated through the C-terminus Thr carboxylate group (in bidentate mode) , and the other two are forming a five-membered chelate with amine and oxo group via N-terminus Gly residue (figure 2.5a). This MBioF is soluble in water and non-soluble is organic solvents such as, ethanol, methanol, and acetone.

Methanol guest molecules can be evacuated by heating the framework up to 100°c under vacuum overnight. According to TGA of [Zn(GlyThr)$_2$].MeOH, the first weight loss occurs at temperatures below 50 ^{o}C which, corresponds to methanol removal. The structure remains stable up to 250°C. The first decomposition of the framework takes place in temperature range of 250-380°C, and the second decomposition occur around 500°C, which corresponds, to the formation of ZnO (figure 2.6).
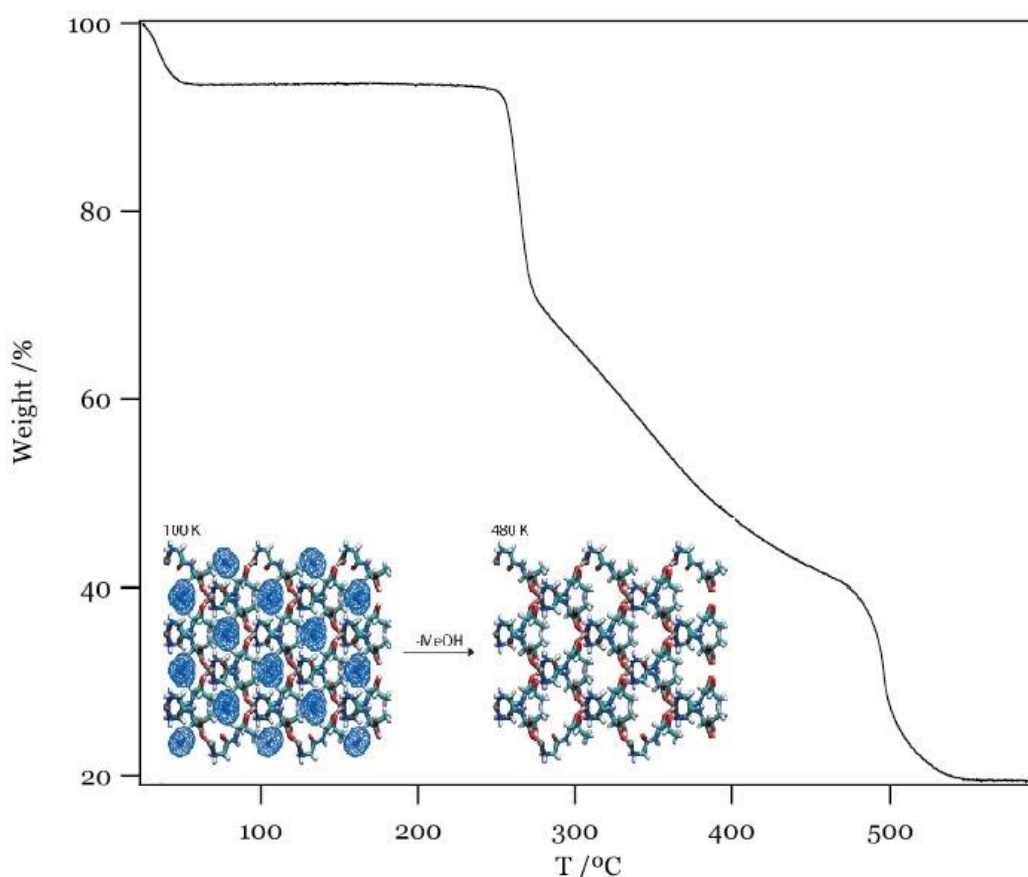
Figure 2.6- Thermogravimetric analysis of [Zn(GlyThr)2].MeOH. Reprinted with permission from[33], Copyright 2012 Wiley-VCH Verlag GmbH & Co. KGaA, Weinheim.

The adsorption isotherm of this framework was fitted to BET theory to get the BET surface area of 192 $m^2.g^{-1}$. The most interesting point of this framework is its adsorption selectivity of CO_2 over CH_4. Figure 2.7a shows the preferential CO_2 over CH_4 adsorption with single-component separation ratio of 14:1 (wt%:wt%) at 1 bar. The highest reported $CO_2:CH_4$ separation ratio for MOFs is 24:1 for $[Zn_2(BPDC)_2BPE]$ at 298 K and 1 atm[38].
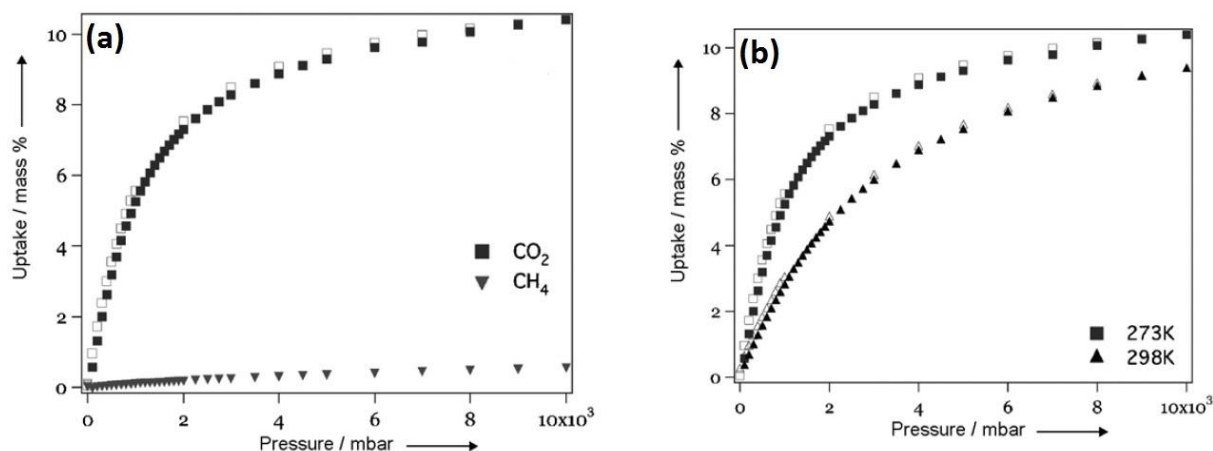
Figure 2.7- (a) Selective sorption of CO_2 (squares) over CH_4 (triangles) of $[Zn(GlyThr)_2].MeOH$ at 273 K. **(b)** CO_2 sorption isotherms of $[Zn(GlyThr)_2].MeOH$ at 273 K (squares) and 298 K (triangles). Filled and empty symbols showing the adsorption and desorption, respectively. Reprinted with permission from[33], Copyright 2012 Wiley-VCH Verlag GmbH & Co. KGaA, Weinheim.

2.3. Tripeptide-based MBioFs

Up to date, there are only two reported tripeptide-based metal-organic frameworks by Lee and co-workers on 2007. They assembled two MBioFs with Cd(II) metal ions and AlaAlaAla and GlyGlyGly tripeptides, structures of these two tripeptides are presented in figure 2.8.
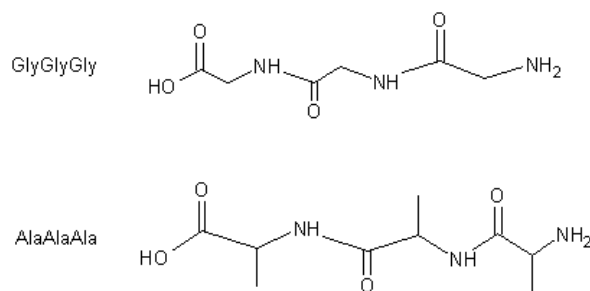
Figure 2.8- Representation of the structures of GlyGlyGly (top) and AlaAlaAla (bottom) tripeptides.

[Cd(GlyGlyGly)$_2$].H$_2$O:

The synthesis route of this framework is similar to earlier reported synthesis for [Cd(AlaThr)$_2$].4H$_2$O. A solution of 0.05 mmol of CdAc$_2$ and 0.10 mmol of GlyGlyGly in 2:2:3 mL of DMF, water, and ethanol, respectively, was sonicated for 5 min with gentle shaking at 150 w using ultrasonic bath. This solution was placed in a 5 mL glass vial, which was in turn was placed in a 20 mL screw-capped vial. One milliliter of 2% triethylamine in ethanol solution was added to the 20 mL vial and sealed with a cap. Needle crystals with 59% yield (based on cadmium) were grown after about 3 months.

The crystalline framework of this MBioF was monoclinic belonging to the space group C2/c. Each octahedral Cd(II) ion was linked to six peptides to form a 3-D complex (figure 2.9a); two of which through the N-terminus of two peptides (monodentate), and four via the C-terminus carboxylates of four peptides (monodentate).
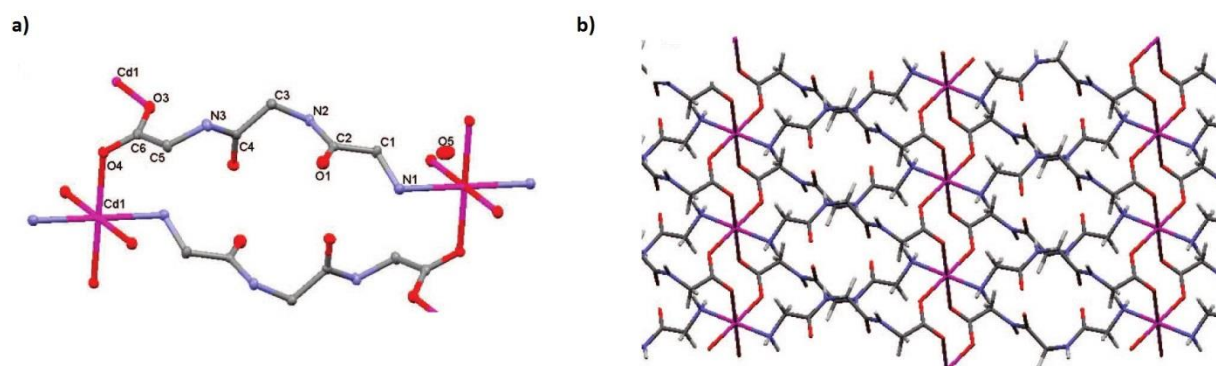
Figure 2.9- (a) Structure of [Cd(GlyGlyGly)$_2$].H$_2$O, showing a 3-D coordination of cadmium ions. **(b)** View along the c axis, showing an 8-membered rings formed by linking two Cd ions to two carboxylate groups. Reprinted with permission from [34], Copyright 2008 American Chemical Society.

[Cd(AlaAlaAla)$_2$]:

This framework was also assembled through the base diffusion method with ultrasound assistant described for [Cd(AlaThr)$_2$].4H$_2$O and [Cd(GlyGlyGly)$_2$].H$_2$O. A solution of 0.15 mmol of CdAc$_2$ and 0.15 mmol of GlyGlyGly in 10:10:5 mL of DMF, water, and ethanol, respectively, was sonicated for 5 min with gentle shaking at 150 w using ultrasonic bath. This solution was placed in a 20 mL glass vial, which was in turn was placed in a 100 mL screw-capped jar. Ten milliliter of 2% triethylamine solution was added to the 100 mL jar and sealed with a cap. Colorless transparent needle crystals with 43% yield were grown after about 3 weeks.

This framework crystallized as monoclinic crystals belonging to the chiral group space *C*2. The resulting framework had a 3-D topology with 1-D pores along its *b* axis. Each Cd(II) ion was octahedrally coordinated by four trialanine peptides; two through the C-terminus carboxylate group of two peptides (monodentate), two other through the N-terminus amine group of two peptides, and finally the remaining two via N-terminus amide carbonyl group of the two other peptides (figure 2.10a).
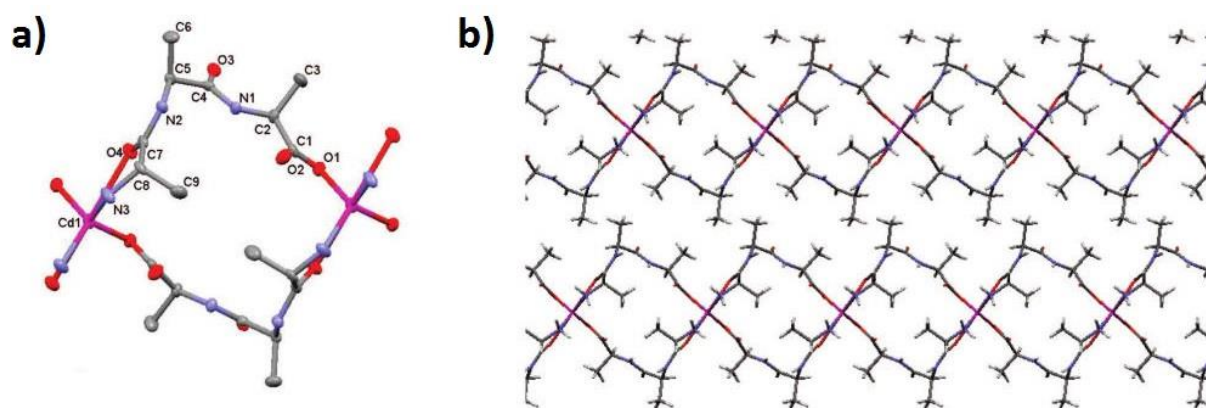
Figure 2.10- **(a)** Structure of [Cd(AlaAlaAla)₂]. **(b)** View along the b axis, exhibiting 1-D pores. Reprinted with permission from [34], Copyright 2008 American Chemical Society.

Chapter 3

3.   Experimental procedure and results

3.1.   Synthesis routes

Two different synthesis routes were applied to assemble metal-peptide framework (MPF) of this work, solvothermal and base diffusion methods. These two methods carried out for assembling MPF of GlyAsp peptide as ligand and Zn(II) ions as metal linker. Different conditions were applied to obtain crystalline material suitable for X-ray diffraction and as a result solvothermal method found to be more convenient than base diffusion method for this work.

Base diffusion method:

1. A solution of 0.05 mmol of $Zn(NO_3)_2.4H_2O$ and 0.1 mmol of GlyAsp in 1.5 mL of water was mechanically stirred for 30 minutes.
2. The solution was basified by adding aqueous NaOH 1M. Four solutions with pH= 5, 6, 7, and 8 were prepared.
3. Each basified solution was placed in a 2 mL glass vial, which was in turn placed in a 20 mL scintillation vial.
4. Two milliliters of methanol was added to the 20 mL scintillation vial and sealed with a cap (figure 3.1).

After about 2 weeks, white amorphous particles were grown in samples with pH of 6 and 7. The resulting materials were not crystalline therefore, not suitable for XRD.

Base diffusion method, is the simplest way to obtain crystalline material but commonly this process needs a long time to complete. Therefore, we moved to other synthesis methods and no more experiments were performed through this route.
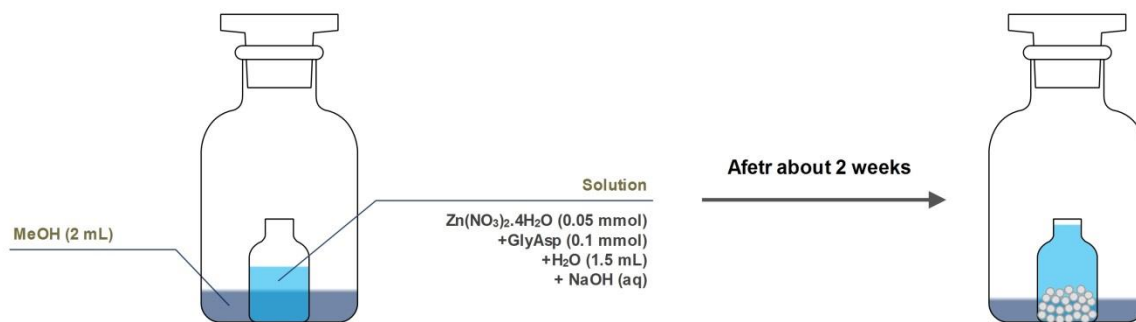
Figure 3.1- Schematic representation of base diffusion method.

Solvothermal method:

This synthesis route is widely used for assembling MPF. As described in chapter 2, metal-peptide frameworks such as [Zn(GlyAla)$_2$].(solvent)[33], and [Zn(GlyThr)$_2$].MeOH[35] were synthesized through this method. Several parameters, such as the reaction time, temperature, stoichiometry, pH, additives, etc. can affect this method.

Several experiments have done with different conditions during this work. Different condition of pH, reaction time, temperature and solvent (table 3.1) were carried out to obtain crystalline particles suitable for further analysis by X-ray diffraction.

- The solvent was chosen to be methanol at first place, but GlyAsp is non-soluble in this organic solvent. Therefore, a mixture of water and methanol was selected, since GlyAsp is soluble in water.

- For all experiments, solutions containing two equivalents of the dipeptide GlyAsp and one equivalent of zinc nitrate tetrahydrate in solvent were stirred for 30 minutes.

- Aqueous sodium hydroxide was added to solutions while stirring, to adjust different pH. For pH higher than 5, white precipitation of Zn(OH)$_2$ were formed. These undesired particles were removed via centrifuge.

- Different reaction time and temperature were tested to find the optimum condition.

During one of these experiments crystalline material formed right after addition of water to reagents (without stirring) this crystal was collected from the solution and its X-ray diffraction showed that the crystal was pure GlyAsp (figure 3.2).

Table 3.1- Selected conditions of the experiments done through solvothermal synthesis method.

Solvent (v/v%)	pH	Temperature (°C)	Reaction time (h)
3.8 mL (50% methanol and 50 %water)	4.74, 4.97, 7.08, 8.10	85	11
3.8 mL (55% methanol and 45% water)	4.39, 6.58, 5.16, 6.05	85	11
3.8 mL (50% methanol and 50 %water)	4.5, 4.76, 4.98, 5.26, 5.57, 5.85	85	15
3.8 mL (50% methanol and 50 %water)	5.49, 6.00, 6.57, 6.97	85	48
3.8 mL (100% water)	6.01, 6.49	85	48
4 mL (60% methanol and 40% water)	5.69	130	12
4 mL (60% methanol and 40% water)+ 4µl pyridine	5.5	95	12
4 mL (50% methanol and 50% water)+ 2µl pyridine	5.6	85	56
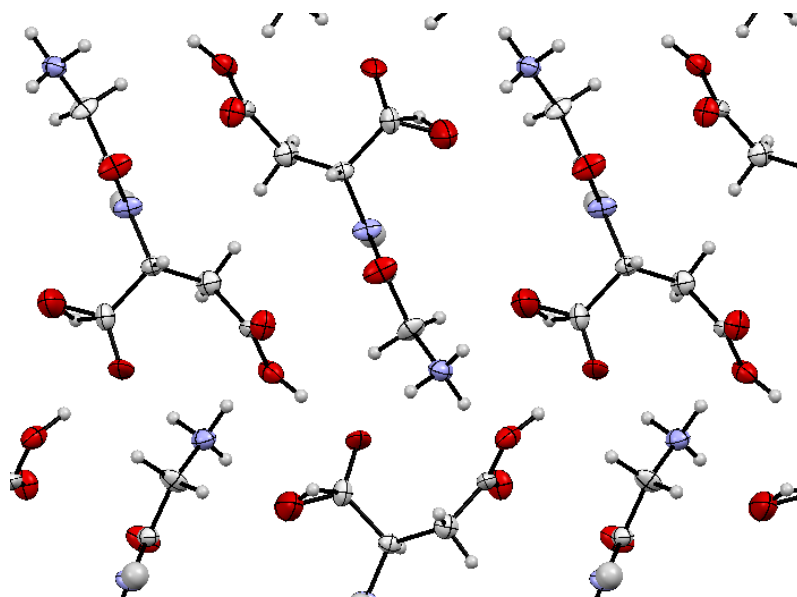
Figure 3.2- Structure of GlyAsp crystal, oxygen (red), nitrogen (light blue), carbon (white), and hydrogen (light grey).

Some of the resulting materials were crystalline but most of the crystals were too small to be collected for X-ray diffraction except one sample. The conditions for **sample A** was 1.9:1.9 mL water and methanol, respectively as solvent, pH 5.57, reaction temperature of 85°C, and reaction time of 15 hours. Detailed experimental procedure of this condition is presented later on section 3.1.1.

X-ray microanalysis is the process of using characteristic X-rays, generated in a sample by electron beam, to determine the composition of the sample. There are two kinds of X-ray microanalysis:

i.   Wavelength Dispersive Spectrometry (WDS), in which wavelength of X-rays are used.
ii.   Energy Dispersive Spectrometry (EDS), in which energy of X-rays are used.

Since the crystalline particles of **sample A** were difficult to collect for X-ray diffraction analysis, first we made EDS microanalysis of this sample to ensure that the material contains zinc in its structure.

Element	Wt %
C	37.65
N	11.03
O	26.37
Zn	24.95
Total	100
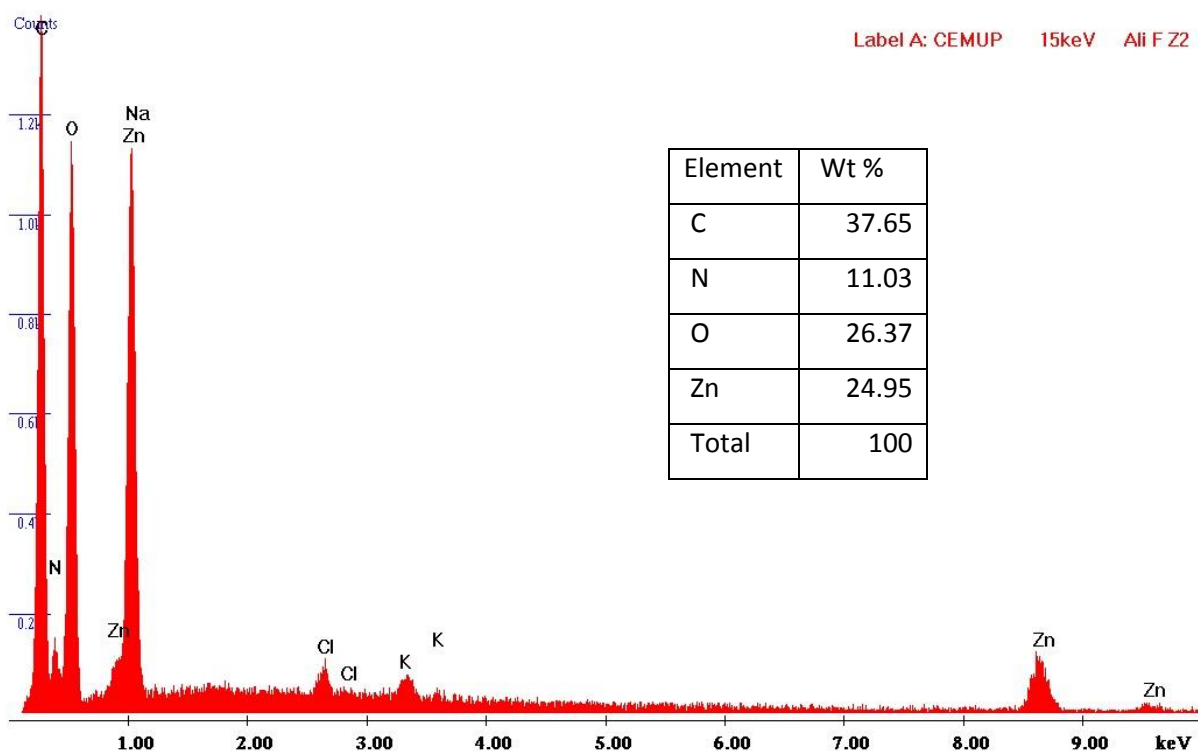
Figure 3.3- Energy dispersive spectrometry analysis of **sample A**.

As shown in figure 3.3, the EDS analysis of **sample A** indicates the presence of the Zn inside the structure of this material. Furthermore, the elemental analysis by EDS showed a decent agreement with the final composition of the sample analyzed by XRD (i.e. C 26.54%, H 3.71%, N 10.32%, O 35.35%, and Zn 24.08%).

3.1.1. Synthesis of [Zn(GlyAsp)].H$_2$O

Here we describe the assembly of MPF [Zn(GlyAsp)].H$_2$O (**1**) through solvothermal method.

A 20 mL scintillation vial was charged with GlyAsp (0.1 mmol, ≥99.0% from Aldrich) and zinc nitrate tetrahydrate (0.05mmol, from Merck) in a water/methanol mixture (1.9/1.9 mL respectively). The following steps carried out to prepare the solution:

1. 0.0130 g (equal to 0.05 mmol) of zinc nitrate was carefully weighted and charged to flask.
2. 0.0190 g (equal to 0.1 mmol) of GlyAsp was added to scintillation vial.
3. 1.9 mL of methanol and 1.9 mL of deionized water was added.
4. The solution was stirred for approximately 30 min.
5. 1 M aqueous sodium hydroxide was added to basify the solution. The pH was adjusted to 5.57 while stirring.
6. Zn(OH)$_2$ precipitation had removed from the solution via centrifuge.
7. Clear solution (without Zn(OH)$_2$) is delivered to a new clean 20 mL vial .
8. The reagents were heated at 85 ^{o}C for 15 hours, and cooled down to room temperature.

Microscopic image of **1** is shown on figure 3.4a which, shows needle shaped crystal with yield of 5.89%[13] (based on zinc) in the edge of the synthesized powders. Scanning Electron Microscope (SEM) image of **1** in scale of 200 μm is displayed on figure 3.4b.
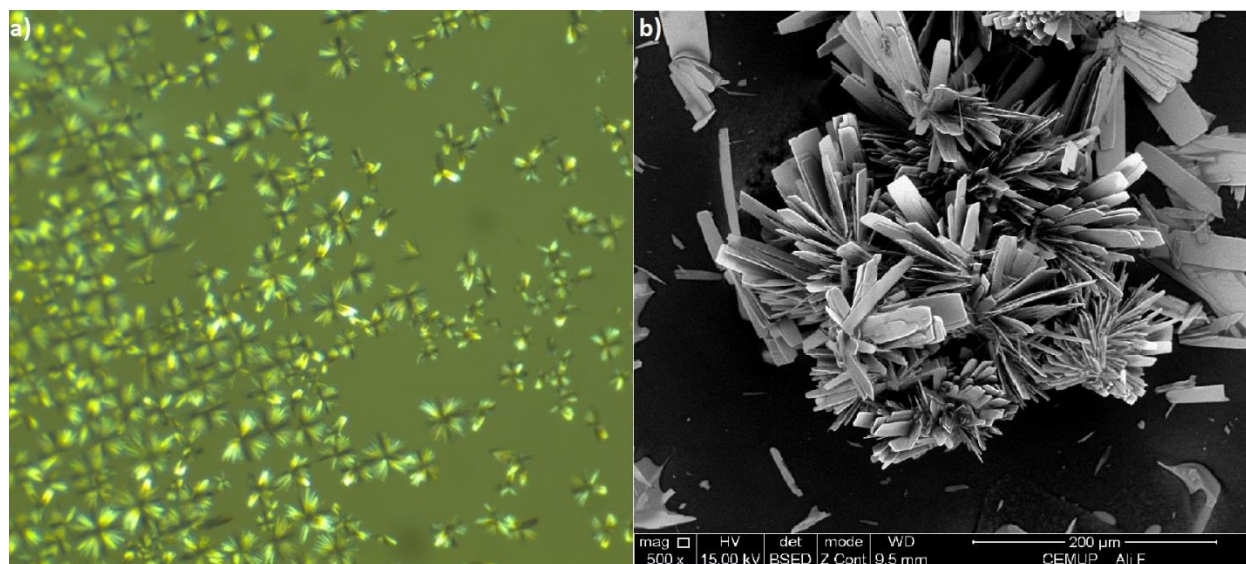
Figure 3.4- **(a)** Microscopic and **(b)** SEM images of [Zn(GlyAsp)].H$_2$O.

---

[13] The yield for final solution (without Zn(OH)$_2$) precipitation was 27.36%

[Zn(GlyAsp)].H$_2$O demonstrate 1:1 stoichiometry of zinc and dipeptide in the framework. Therefore, another way to synthesis of this material is to use 1:1 stoichiometry of dipeptide and zinc salt. This new synthesis route can reduce the amount of dipeptide used and thus reducing the final cost of framework assembly of **1**.

3.1.2. Synthesis of [Co(GlyAsp)].H$_2$O

We used a similar solvothermal synthesis method to assemble cobalt-based peptide framework. Thus instead of zinc salt, cobalt nitrate salt is used for synthesis of MPF [Co(GlyAsp)].H$_2$O (**2**).

A 20 mL scintillation vial was charged with GlyAsp (0.1 mmol, ≥99.0% from Aldrich) and cobalt (II) nitrate hexahydrate (0.05mmol, 98% from Sigma-Aldrich) in a water/methanol mixture (1.9/1.9 mL respectively). The following steps carried out to prepare the solution:

1. 0.0145 g (equal to 0.05 mmol) of cobalt nitrate salt was carefully weighted and charged to flask.
2. 0.0190 g (equal to 0.01 mmol) of GlyAsp was added to scintillation vial.
3. 1.9 mL of methanol and 1.9 mL of deionized water was added.
4. The solution was stirred for approximately 45 min. A transparent (with pink color) and clear solution had reached.
5. 1 M aqueous sodium hydroxide was added to basify the solution. The pH was adjusted to 5.99 while stirring.
6. The reagents were heated at 85 °C for 15 hours, and cooled down to room temperature for 30 min (the sample left in the oven to cool down to room temperature for about 5 hours).

As shown in figure 3.5a, needle shape crystals were grown in the edge of powders of **2**.
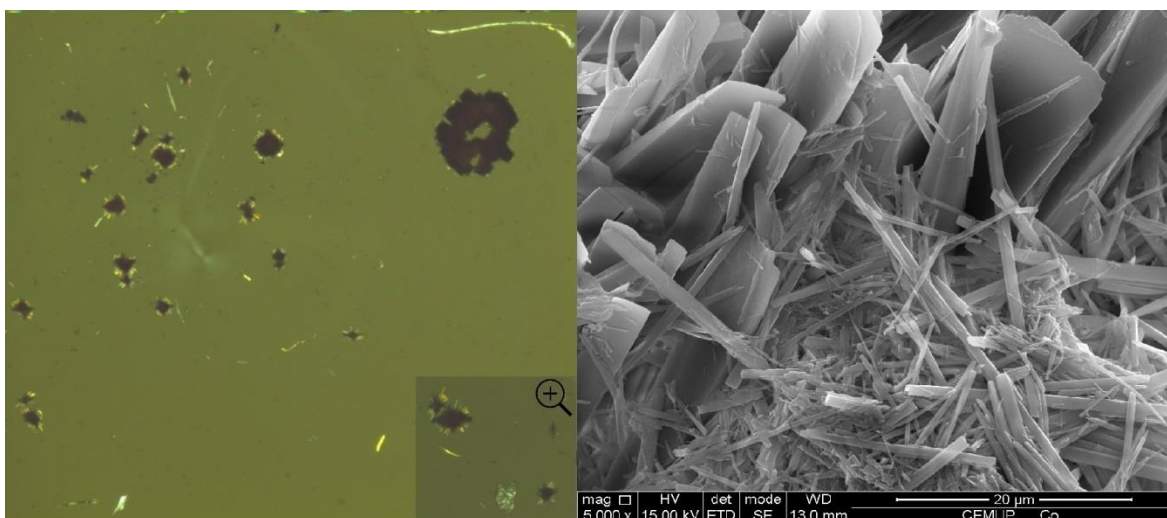
Figure 3.5- **(a)** Microscopic and **(b)** SEM images of [Co(GlyAsp)].H$_2$O.

Comparing to **1**, this framework has advantages such as, no undesired precipitation of cobalt hydroxide during assembly, and higher crystal yield (22.23% based on cobalt). In contrast, although the framework of **2** has 1:1 stoichiometry of dipeptide and Co but the yield of crystallization was highly decreased when this stoichiometry was applied thus, 1:1 stoichiometry is not suitable for assembly of this framework.

3.2. X-ray diffraction

X-ray diffraction (XRD) is a method used for determining the structure of a crystal. When X-ray beams interact with crystalline substance, they diffract and as a result, a diffraction pattern is obtained. Every crystalline substance gives a unique pattern therefore, XRD pattern of a pure substance is like a fingerprint of the substance. By measuring the angle and intensity of diffracted X-ray beams, the structure of crystal can be solved.

Table 3.2 shows the crystal data and structure refinement for **1** and **2**.
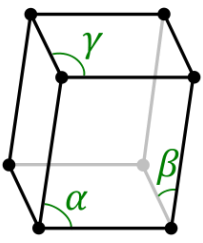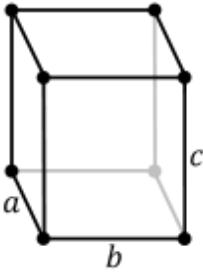
Table 3.2- Crystal data and structure refinement for $[Zn(GlyAsp)].H_2O$ and $[Co(GlyAsp)].H_2O$.

Metal-peptide framework	$[Zn(GlyAsp)].H_2O$	$[Co(GlyAsp)].H_2O$
Empirical formula	$C_6H_{10}N_2O_6Zn$	$C_6H_9N_2O_6Co$
Formula weight (g/mol)	271.54	264.09
Temperature (K)	100	120
Crystal system	Monoclinic	Orthorhombic
Space group	$P2_1$	$P2_12_12_1$
a (Å)	4.807	6.086
b (Å)	9.472	8.954
c (Å)	9.701	16.757
α (°)	90	90
β (°)	95.76	90
γ (°)	90	90
Volume (Å^3)	439.5	913.17
Z	2	4
ρ_{cal} (g/cm^3)	2.0519	1.9135
R indexes[14] (all data)	R1=0.0676 , wR2=0.1694	R1=0.0693 , wR2=0.1687

---

[14] R1=$\sum$||F_o|-|F_c||/$\sum$|F_o| and wR2= [w(F_o^2-F_c^2)^2]/[w(F_o^2)^2]$^{1/2}$.

As reported in table 3.2, crystals system of **1** and **2** are monoclinic and orthorhombic, respectively. Both of these frameworks have primitive (P) lattice centering, in which lattice points are only coordinated on the cell corners. Space group describes the symmetry of a crystal, and Z value indicates the number of the symmetry operators (table 3.3).

Table 3.3- Lattice shape and symmetry operators for [Zn(GlyAsp)].H$_2$O and [Co(GlyAsp)].H$_2$O.

Metal-peptide framework	[Zn(GlyAsp)].H$_2$O	[Co(GlyAsp)].H$_2$O
Crystal system	Monoclinic	Orthorhombic
Lattice shape	$\beta \neq 90°$ $\alpha, \gamma = 90°$	$a \neq b \neq c$
Space group	P2$_1$	P2$_1$2$_1$2$_1$
Symmetry operators	(x,y,z) (-x,y+1/2,-z)	(x,y,z) (1/2-x,-y,1/2+z) (-x,1/2+y,1/2-z) (1/2+x,1/2-y,-z)

3.3. Structure

Here we describe the structures and metal coordination modes for **1** and **2**. Both of these frameworks were assembled with GlyAsp dipeptide ligands. The structure of GlyAsp illustrated in figure 3.6.
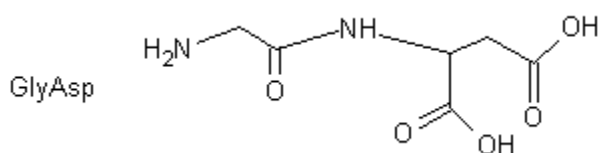
Figure 3.6- Representation of the structure of GlyAsp.

As mentioned before, two different metal salts of zinc and cobalt nitrates were used for synthesis of these frameworks. Coordination modes for Zn (II) and Cobalt (II) metal ions in frameworks **1** and **2** are presented in figure 3.7.
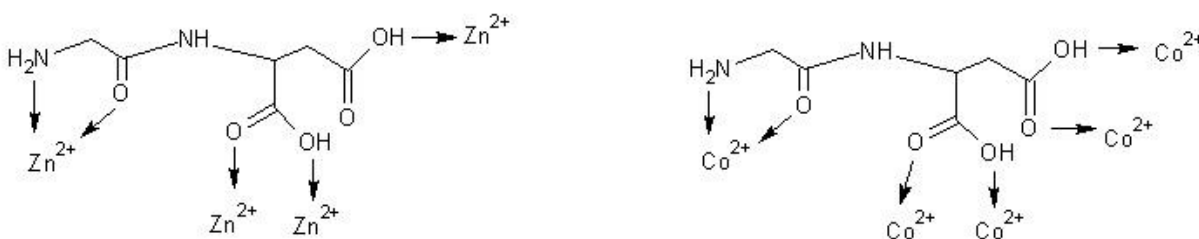
Figure 3.7- Metal ions coordination modes for [Zn(GlyAsp)] (left) and [Co(GlyAsp)] (right).

3.3.1. Structure of [Zn(GlyAsp)].H₂O

As shown in figure 3.7, four Zn(II) metal ions are linked to each GlyAsp dipeptide. Each pentahedral Zn(II) ions are linked to four other metal ions by four dipeptide ligands; one forming a five-membered chelate with amine and oxo group through N-terminus Gly residue, two through C-terminus carboxylate group of Asp α-carbon (in bidentate mode), and finally one via C-terminus carboxylate group of β-carbon of Asp residue (monodentate). Therefore, adapting tetradentate coordination mode of μ_4-N_1O_1:O_2:O_3:O_4 (figure 3.8).
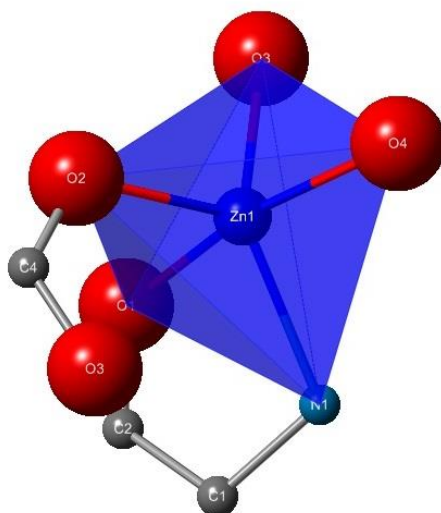
Figure 3.8- Representation of Zn(II) ion coordination in [Zn(GlyAsp)].

The framework of **1** exhibits 2-D topology with 1-D pores along the *a* axis. Figure 3.9 illustrates the extended structure of **1**, in which the solvent molecules (water) are placed in channels of the framework. These solvent molecules can be removed by heating up to 100°C.
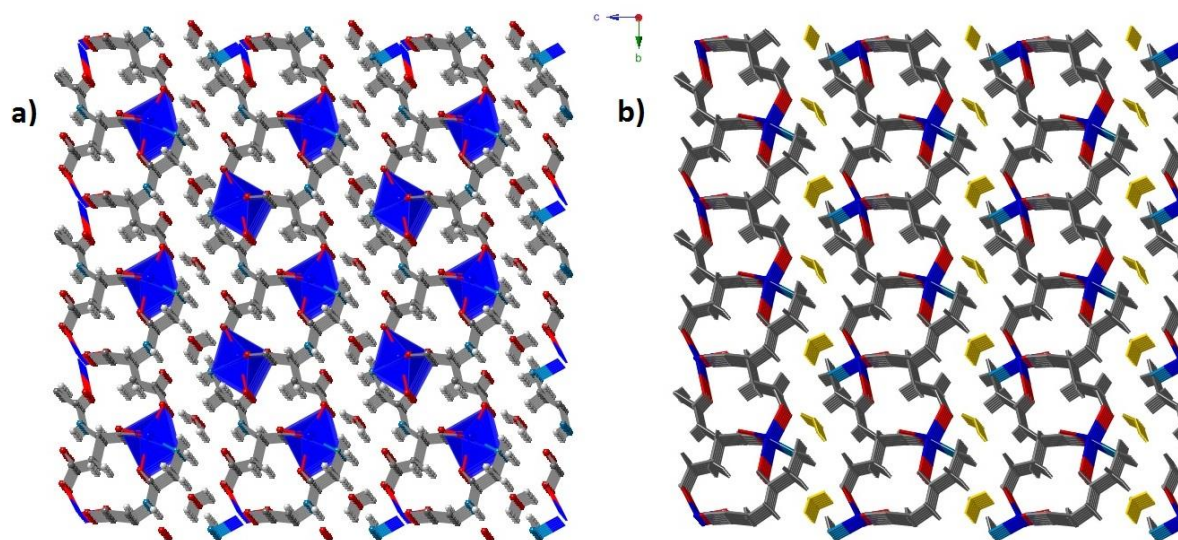
Figure 3.9- Structure of [Zn(GlyAsp)].H$_2$O; **(a)** Polyhedral representation, zinc (blue polyhedral), hydrogen (white), carbon (grey), oxygen (red), and nitrogen (light blue). **(b)** Stick representation, Zn-N bond (blue-light blue), Zn-O bond (blue-red), and water molecules (yellow).

3.3.2. Structure of [Co(GlyAsp)].H$_2$O

Five cobalt (II) metal ions are coordinated with each GlyAsp dipeptide (figure 3.7). Each octahedral Co(II) ions are bridged to five other metal ions by five dipeptide ligands; one forming a five-membered chelate with amine and oxo group through N-terminus Gly residue, four via C-terminus carboxylate group of Asp α and β-carbons (each two in bidentate mode). As a result, adapting pentadentate coordination mode of μ_5-N$_1$O$_1$:O$_2$:O$_3$:O$_4$:O$_5$ (figure 3.10c).

Compound **2**, shows three-dimensional porous structure, which has one-dimensional pores along *a* axis. These pores are filled with water guest molecule. As mentioned earlier in chapter 2, metal-peptide frameworks commonly have 1-D topology and a few of them showing 2-D structure, 3-D topologies are scarce.

Figure 3.10 represents the structure of this framework in two models of polyhedral and sticks. The five-membered chelate ring formed through the N-terminus of Gly is clearly shown in the stick model.
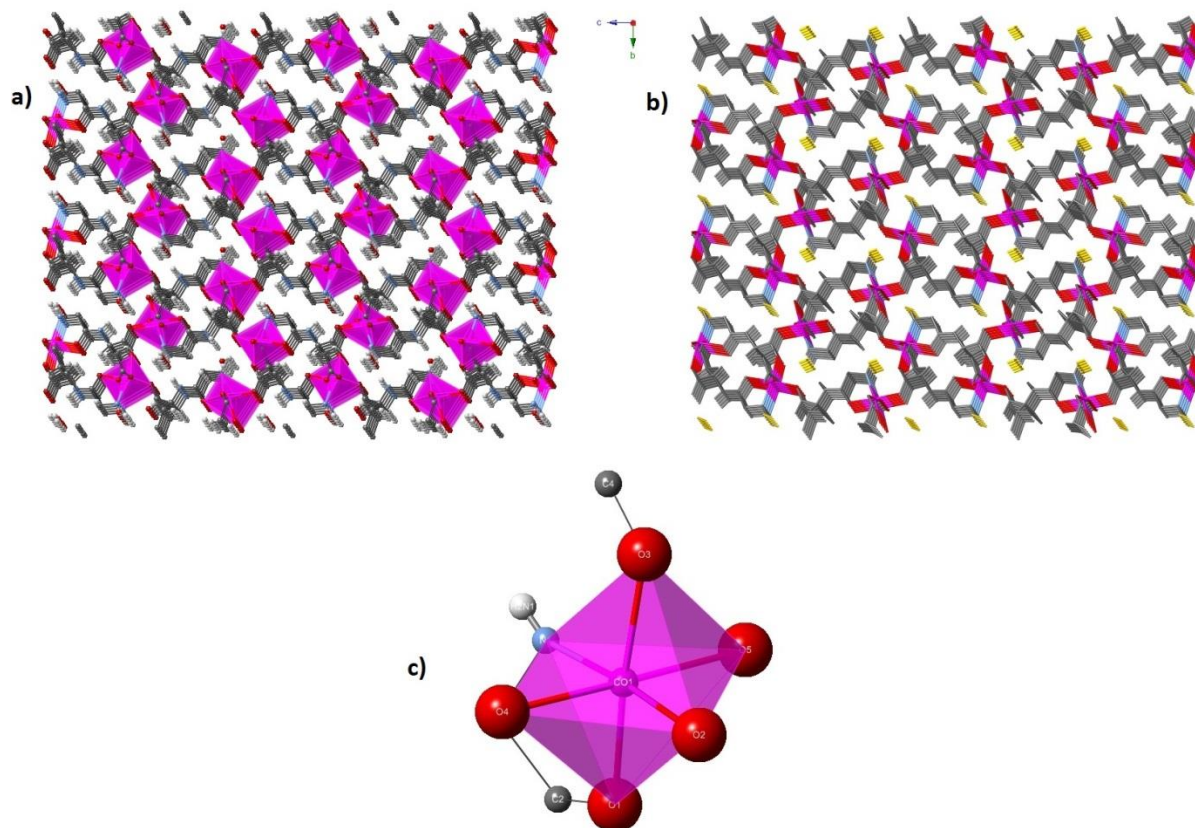
Figure 3.10- Structure of [Co(GlyAsp)].H$_2$O; **(a)** Polyhedral representation, cobalt (pink polyhedral), hydrogen (white), carbon (grey), oxygen (red), and nitrogen (light blue). **(b)** Stick representation, Co-N bond (pink-light blue), Co-O bond (pink-red), and water molecules (yellow). **(c)** Octacoordinated Co(II) ions in [Co(GlyAsp)].H$_2$O complex.

3.4. Thermogravimetric analysis

Thermogravimetric analysis (TGA) is the analysis of weight changes in relation to changes in temperature. A plot of weight loss versus temperature exhibits the composition changes in sample and thermal stability of referred sample. Another curve of derivative weight loss (DTG) can be used to see the point at which weight loss is most apparent.

TGA of compounds **1** and **2** were carried out with NETZSCH TG 209 F1 instrument in 30-650°C temperature range with heating rate of 5°C.min^{-1} and air flow rate of 50 mL.min^{-1}. Sample size of 11 and 21 mg of framework **1** and **2** used for these measurements.

3.4.1. Thermogravimetric analysis of [Zn(GlyAsp)].H$_2$O

Figure 3.11 displays the TGA of metal-peptide framework of **1**. The first weight loss, corresponded to the removal of water guest molecules, takes place at temperature below 100 ^{o}C. This 6.5% weight loss is in good agreement with 6.6% water molecule fraction in the framework of compound **1**. The framework remains stable up to 250 ^{o}C where the second decomposition occurs. Finally, weight loss of 69% at temperature of 500°C, which leaves a final residue with molar weight of 84.12 g.mol^{-1} associated with the formation of Zn(II) oxide[15].
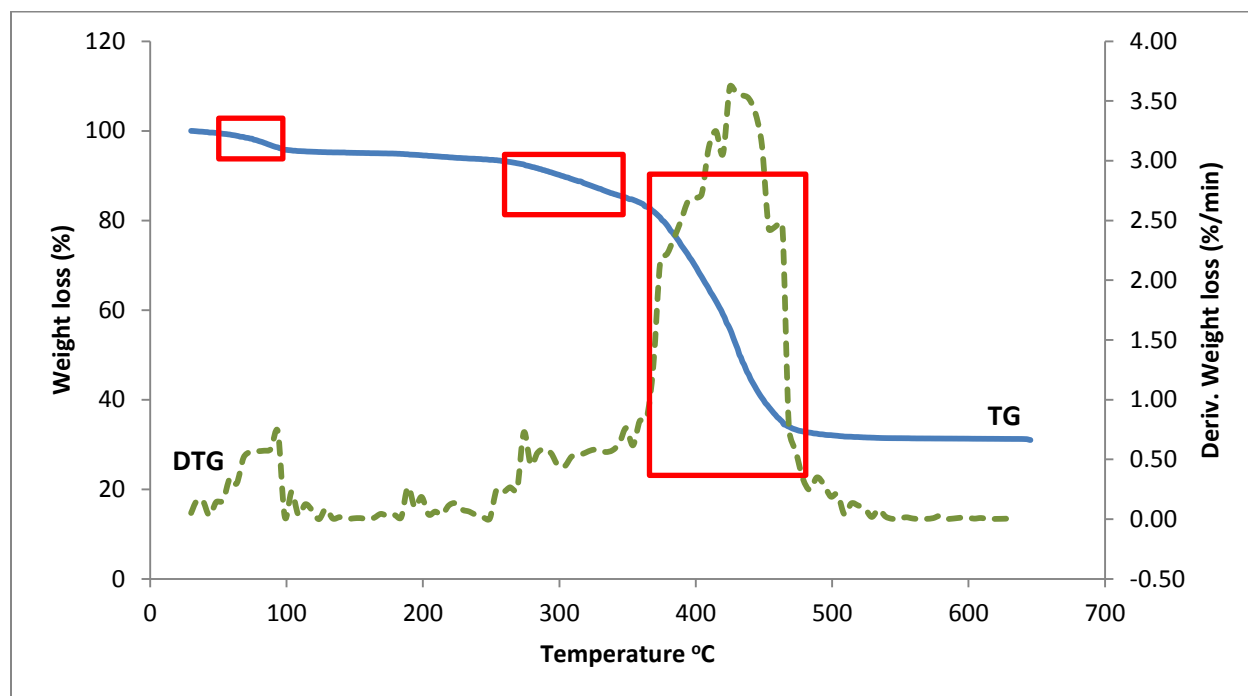
Figure 3.11- Thermogravimetric analysis of [Zn(GlyAsp)].H$_2$O (blue solid line). Green dashed line indicates the derivative weight loss (right-hand scale), and apparent weight losses are highlighted with red boxes.

3.4.2. Thermogravimetric analysis of [Co(GlyAsp)].H$_2$O

This framework exhibits different decomposition behavior comparing to framework **1**. As shown in figure 3.12, the first decomposition occurs at temperature range of 115-240 ^{o}C with 6.15% weight loss that is associated to water removal. Decomposition continues up to 350°C where fast weight loss takes place through 30°C temperature increase. The final 69.89% weight loss after 380°C is in sufficient agreement with formation of Co(II) oxide[16].

---

[15] ZnO=81.39 g.mol^{-1}
[16] CoO=74.93 g.mol^{-1} approximately equal to 79.78 g.mol^{-1} (residue molar weight)

As mentioned in section 3.2.2, pores of this framework are filled with these guest molecules therefore; better adsorption behavior can accomplish after evacuation by heating the framework of **2** up to 240°C.
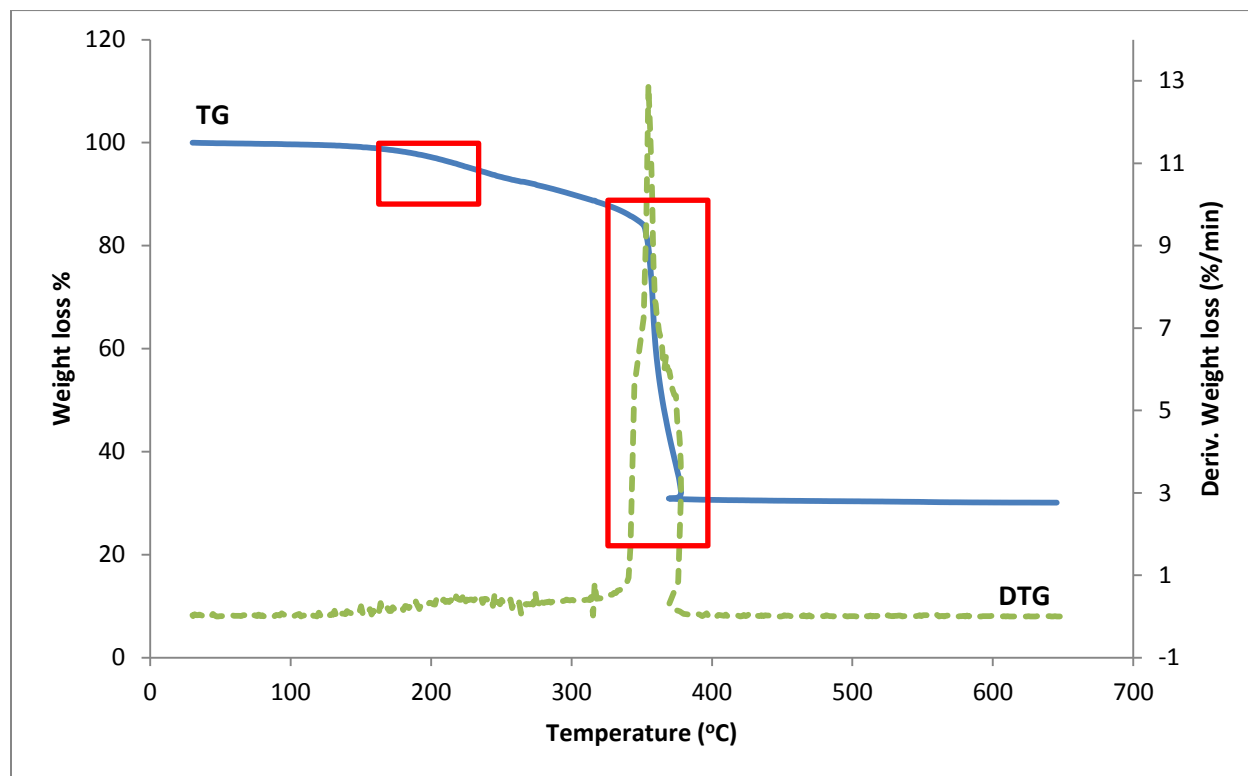
Figure 3.12- Thermogravimetric analysis of [Co(GlyAsp)].H$_2$O (blue solid line). Green dashed line indicates the derivative weight loss (right-hand scale), and apparent weight losses are highlighted with red boxes.

3.5. Adsorption

Every sorption process is consist of two components, sorbate and sorbent. Fluid phase (sorbate) is transferred to sorbing agent (sorbent) which could be suspended in a vessel or packed in a column[39].

Adsorption, ion exchange, and chromatography are sorption operations. In an adsorption process, sorbate (gas/liquid) diffuses to the surface of a sorbent (solid). Molecules, atoms, or ions of sorbate bond with the surface of the sorbate or are held by weak intermolecular forces of it. In general, the solid material is referred to as adsorbent, whereas the adsorbed solutes are called adsorbate. During adsorption, the adsorbent become saturated or nearly saturated with the molecules, atoms, or ions of the adsorbate. The adsorbent is regenerated by desorption the sorbed material, in order to reuse the

adsorbent. As mentioned before, adsorption can be classified as purification or bulk separation, depending on the concentration in the feed fluid of the components to be adsorbed[17] [39].

Different types of forces between adsorbate molecule and the molecules of the adsorbent may categorize adsorption into physical adsorption (van der Waals adsorption) and chemisorption (activated adsorption). Physical adsorption from a gas happens when the intermolecular forces of the gas are smaller than the intermolecular attractive forces between molecules of adsorbent and the gas. The resulting   adsorption is exothermic and it is similar to condensation. Physical adsorption begins as a monolayer, becomes multilayered, and then, if the pores are close to the size of the molecules, capillary condensation occurs, the pores fill with adsorbate. Capacity of a porous adsorbent depends on the pore volume of it. However, in case of having gas for adsorbate and at temperature beyond its critical temperature, physical adsorption is limited to a monolayer. In contrast, chemisorption occurs when adsorbent and adsorbate form a chemical bond with each other. Chemisorption from a gas adsorbate usually happens at temperatures higher than 200 ^{o}C and may be slow and irreversible [39].

3.5.1.   Volumetric method for gas adsorption

During the adsorption of gas in solid, the weight of the solid increases and the pressure of the gas decreases. Therefore, the amount adsorbed can be measured from mass or pressure changes. When the weight change is used for measurement, the technique is referred to as gravimetric adsorption method. Alternatively, measurement based on the gas pressure change is called volumetric adsorption method. In volumetric method, the volume of the sample required for measurement. The equilibrium adsorption isotherm is the plot of pressure versus amount adsorbed at a constant temperature.

A schematic representation of volumetric apparatus used for this work is shown in figure 3.13. Commonly, volumetric apparatuses are consisting of two sides, injection side and sample side. The volumes of these two sides are also required for measurements.

For measuring adsorption at a certain pressure and temperature two steps should carried out. Frist step is to hold the gas inside the injection side while the valve (R_2) between two sides is closed. Second step is followed by opening the R_2 valve, and allowing the gas into the sample side, where the adsorption takes place.

---

[17] Bulk separation (adsorption of 10 wt% or more from adsorbate) and Purification (> 2 wt %)
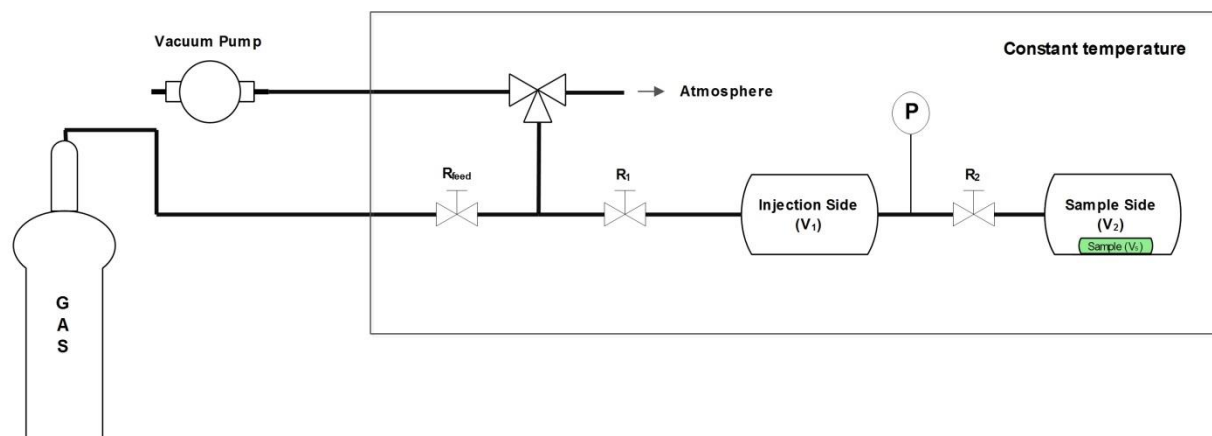
Figure 3.13- Schematic representation of volumetric adsorption apparatus.

The initial pressure inside injection and sample side is set to zero through making vacuum in the whole apparatus. After following those two described steps, the adsorption data for the first pressure point can be collected. For collecting adsorption data for the second pressure point, there are two possible routes. First route is to repeat the procedure through making another vacuum between each pressure point. Alternatively, second route is to continue the procedure without making vacuum, which in this case the final equilibrium pressure of previous point is considered as the initial pressure for the sample side.

In this work, cumulative measurement (second route) is used for data collection. Schematic representation of cumulative adsorption measurement used for two pressure points is shown on figure 3.14. The following calculation should be considered for measuring the amount adsorbed for this method.

$$V_i = V_1$$

$$V_f = V_1 + V_2 - V_s$$

$$n_0 = \frac{P_0(V_2 - V_s)}{RT} \quad if\ P_0 = 0 \ \rightarrow n_0 = 0$$

$$n_{i,x} = \frac{P_{i,x}V_i}{RT}$$

$$n_{f,x} = \frac{P_{f,x}V_f}{RT}$$

$$n_{0,x} = n_{f,x-1} = \frac{P_{f,x-1}V_f}{RT}$$

$$n_{ads"excess",x} = n_{0,x} + n_{i,x} - n_{f,x}$$

$$n_{ads,Total} = \sum_{i=1}^{n} n_{ads"excess",i}$$

P=0

P=P$_{i,1}$

P=P$_{f,1}$

P=P$_{i,2}$

P=P$_{f,2}$

P↑

Open valve

Close valve
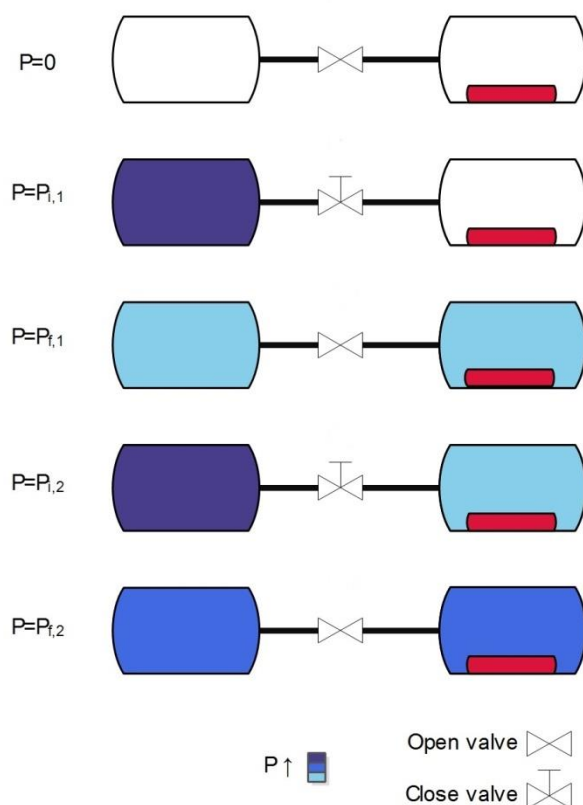
Figure 3.14- Schematic representation of cumulative adsorption data collection for volumetric method.

3.5.2. CO$_2$ equilibrium adsorption isotherm of [Co(GlyAsp)]

Cobalt framework has chosen to be studied for its CO_2 adsorption behavior since the production yield of this MPF was higher than the Zn-based peptide framework. Crystals of [Co(GlyAsp)].H_2O were collected from the containers by removing the solvent (water and methanol mixture) from vials and leaving them at room temperature overnight.

Adsorption of as synthesized [Co(GlyAsp)].H$_2$O showed non-porous behavior of CO$_2$ since water molecules filled the pores of this MPF and leaving no space for CO$_2$ molecule to enter into the pores. Therefore, 96 mg of **2** were heated up to 240 ^{o}C overnight in order to remove the guest molecules. As a result, the evacuated framework showed low CO$_2$ adsorption behavior, which is the evidence of low water removal from the pores. The following procedure was carried out to calculate the amount adsorbed for the first point of CO$_2$ adsorption behavior of this material at 288 K. Table 3.4 shows excess and total CO$_2$ adsorption amount for remaining points.

$$V_i = V_1 = 1.2800 \ cm^3$$

$$V_f = V_1 + V_2 - V_s = 1.2800 + 1.0549 - 0.05017 = 2.28479 \ cm^3$$

$$n_0 = \frac{P_0(V_2 - V_s)}{RT} = \frac{0.0078 \ [bar].(1.0549 - 0.05017)[cm^3]}{0.083145 \left[\frac{cm^3.bar}{K.mmol}\right].288.15 \ K} = 0.000327 \ mmol$$

$$n_{i,1} = \frac{P_{i,1}V_i}{RT} = \frac{0.8041 \ [bar].(1.2800)[cm^3]}{0.083145 \left[\frac{cm^3.bar}{K.mmol}\right].288.15 \ K} = 0.04296 \ mmol$$

$$n_{f,x} = \frac{P_{f,x}V_f}{RT} = \frac{0.444 \ [bar].(2.28479)[cm^3]}{0.083145 \left[\frac{cm^3.bar}{K.mmol}\right].288.15 \ K} = 0.042343 \ mmol$$

$$n_{ads"excess",1} = n_{0,1} + n_{i,1} - n_{f,1} = 0.000327 + 0.04296 - 0.042343 = 0.000945 \ mmol$$

$$q = \frac{n_{ads}}{m_{adsorbent}} = \frac{0.000945 \ [mmol]}{0.096 \ [g]} = 0.009843 \ mol.kg^{-1} \times 0.04401 \ \frac{kg \ CO_2}{mol \ CO_2} \times 100$$

$$= 0.43311 \ \%wt$$

Table 3.4- CO$_2$ amount adsorbed for [Co(GlyAsp)].H$_2$O at 288 K.

P (bar)	n ads, excess	n ads, total	q (mol.kg^{-1})	q (%wt)
0.444	0.000945	0.000945	0.009843	0.043311
0.9285	0.000811	0.001756	0.018287	0.080464
1.523	0.000872	0.002628	0.027372	0.120435
2.503	0.001187	0.003814	0.039732	0.174821
3.244	0.000712	0.004526	0.047146	0.207443

The CO_2 adsorption isotherm of **2** is shown on figure 3.15 which shows low adsorption uptake that can be compared to the CH_4 adsorption behavior of $[Zn(GlyThr)_2]$ metal-peptide framework. This isotherm is well fitted to Freundlich adsorption isotherm.
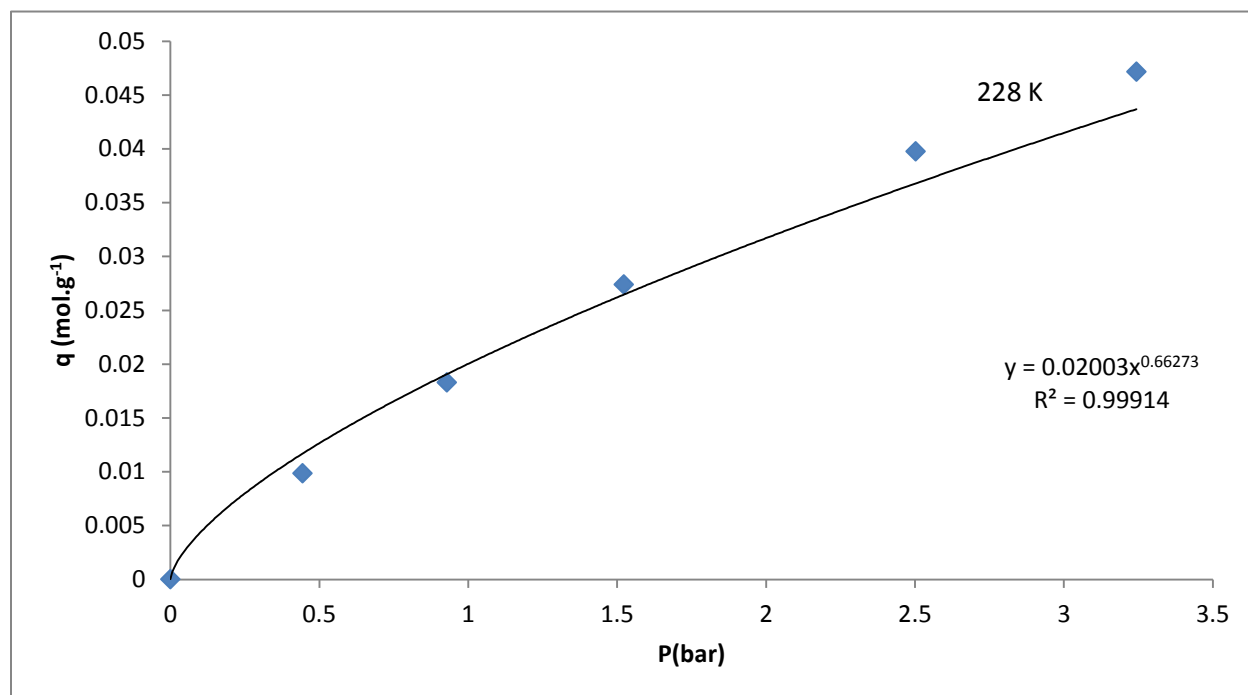

Figure 3.15- CO_2 adsorption isotherm of $[Co(GlyAsp)].H_2O$ at 288 K.

Chapter 4

4.   Conclusions

This work was challenging project since metal-dipeptide frameworks are very hard to crystallize. Perhaps the most notable frameworks of this class of materials are [Zn(GlyAla)$_2$] and [Zn(GlyThr)$_2$], which was reported by Rosseinsky group in *Science* and *Angew Chemie* journals. Therefore, similar synthesis route was followed for assembling MPFs of this work.

Crystallization trials are time consuming and several conditions come into factor if crystals are grown or not. Some of these factors include pH, reaction temperature, reaction time, solvent used and concentration of the reagents. Moreover, due to the flexibility and to the variations of the properties of the dipeptides the crystallization conditions are unique for each one and very challenging to obtain.

Two assembled framework were reported on this work. MPF formulated as [M(GlyAsp)].H$_2$0 (where M is Zn(II) or Co(II)), which exhibit different topologies. Zn-based framework showed two-dimensional structure, which is common for dipeptide-based frameworks. In contract, Co-based framework displays three-dimensional topology, which is rare for these types of materials. To our knowledge, the only reported 3-D structure constructed by dipeptide is [Cd(GlyGlu)$_2$].3H$_2$O (Ferrari et al. 2002).

Single crystal X-ray diffraction, thermogravimetric analysis and scanning electron microscopy gave further insight about the atomic structure, the stability and the morphology of the crystals.

The two related structures of the Rosseinsky group show distinct sorption behavior; while [Zn(GlyAla)$_2$] displays an interesting adaptable structure to the variations of the loading of the guest, the [Zn(GlyThr)$_2$] shows an enhanced rigidity and robustness facilitating the storage; moreover [Zn(GlyThr)$_2$] displays an interesting CO$_2$/CH$_4$ sorption selectivity. However, the CO$_2$ sorption behavior of the cobalt framework of this study showed low uptake since the water guest molecules were trapped inside the pores of this rigid MPF.

Finally, the stability of structures of this work is similar or slightly better than the one of [Zn(GlyThr)$_2$].

References

[1]   R. J. Kuppler, D. J. Timmons, Q.-R. Fang, J.-R. Li, T. a. Makal, M. D. Young, D. Yuan, D. Zhao, W. Zhuang, and H.-C. Zhou, "Potential applications of metal-organic frameworks," *Coordination Chemistry Reviews*, vol. 253, no. 23–24, pp. 3042–3066, Dec. 2009.

[2]   I. Imaz, M. Rubio-Martínez, J. An, I. Solé-Font, N. L. Rosi, and D. Maspoch, "Metal-biomolecule frameworks (MBioFs).," *Chemical Communications*, vol. 47, no. 26, pp. 7287–7302, Jul. 2011.

[3]   P. Horcajada, R. Gref, T. Baati, P. K. Allan, G. Maurin, P. Couvreur, G. Férey, R. E. Morris, and C. Serre, "Metal-organic frameworks in biomedicine.," *Chemical reviews*, vol. 112, no. 2, pp. 1232–68, Feb. 2012.

[4]   H.-C. Zhou, J. R. Long, and O. M. Yaghi, "Introduction to metal-organic frameworks.," *Chemical reviews*, vol. 112, no. 2, pp. 673–4, Feb. 2012.

[5]   O. M. Yaghi, M. O'Keeffe, N. W. Ockwig, H. K. Chae, M. Eddaoudi, and J. Kim, "Reticular synthesis and the design of new materials.," *Nature*, vol. 423, no. 6941, pp. 705–14, Jun. 2003.

[6]   N. Stock and S. Biswas, "Synthesis of Metal-Organic Frameworks (MOFs): Routes to Various MOF Topologies, Morphologies, and Composites," *Chemical reviews*, vol. 112, pp. 933–969, 2012.

[7]   and J.-S. C. Sung Hwa Jhung, Jin-Ho Lee, "Microwave Synthesis of a Nanoporous Hybrid Material, Chromium Trimesate," *Bull. Korean Chem. Soc*, vol. 26, no. 6, p. 880, 2005.

[8]   A. L.-G. and S. L. J. Anne Pichon, "Solvent-free synthesis of a microporous metal–organic framework," *CrystEngComm*, vol. 8, pp. 211–214, 2006.

[9]   J. H. Bang and K. S. Suslick, "Applications of ultrasound to the synthesis of nanostructured materials.," *Advanced materials*, vol. 22, no. 10, pp. 1039–59, Mar. 2010.

[10]   D. J. Tranchemontagne, J. L. Mendoza-Cortés, M. O'Keeffe, and O. M. Yaghi, "Secondary building units, nets and bonding in the chemistry of metal-organic frameworks.," *Chemical Society reviews*, vol. 38, no. 5, pp. 1257–83, May 2009.

[11]   C. S. Collins, D. Sun, W. Liu, J.-L. Zuo, and H.-C. Zhou, "Reaction-condition-controlled formation of secondary-building-units in three cadmium metal–organic frameworks with an orthogonal tetrakis(tetrazolate) ligand," *Journal of Molecular Structure*, vol. 890, no. 1–3, pp. 163–169, Nov. 2008.

[12]   M. P. Suh, H. J. Park, T. K. Prasad, and D.-W. Lim, "Hydrogen storage in metal-organic frameworks.," *Chemical reviews*, vol. 112, no. 2, pp. 782–835, Feb. 2012.

[13]   J.-R. Li, R. J. Kuppler, and H.-C. Zhou, "Selective gas adsorption and separation in metal-organic frameworks.," *Chemical Society reviews*, vol. 38, no. 5. pp. 1477–504, May-2009.

[14]   K. A. S. JeongYong Lee, Omar K. Farha, John Roberts and S. T. N. and J. T. Hupp, "Metal–organic framework materials as catalysts.pdf," *Chemical Society reviews*, vol. 38, pp. 1450–1459, 2009.

[15]   A. Morozan and F. Jaouen, "Metal organic frameworks for electrochemical applications," *Energy & Environmental Science*, vol. 5, no. 11, p. 9269, 2012.

[16]   M. P. Suh, H. J. Park, T. K. Prasad, and D.-W. Lim, "Hydrogen storage in metal-organic frameworks.," *Chemical reviews*, vol. 112, no. 2. pp. 782–835, 08-Feb-2012.

[17]   O. Zn, S. S. Kaye, A. Dailly, O. M. Yaghi, and J. R. Long, "Impact of Preparation and Handling on the Hydrogen Storage Properties of MOF-5," *J. Am. Chem. Soc*, vol. 129, pp. 14176–14177, 2007.

[18]   D. Farrusseng, S. Aguado, and C. Pinel, "Metal-organic frameworks: opportunities for catalysis.," *Angewandte Chemie (International ed. in English)*, vol. 48, no. 41, pp. 7502–13, Jan. 2009.

[19]   Y. Lu, M. Tonigold, B. Bredenkötter, D. Volkmer, J. Hitzbleck, and G. Langstein, "A Cobalt(II)-containing Metal-Organic Framework Showing Catalytic Activity in Oxidation Reactions," *Zeitschrift für anorganische und allgemeine Chemie*, vol. 634, no. 12–13, pp. 2411–2417, Oct. 2008.

[20]   R. T. Yang, *ADSORBENTS:FUNDAMENTALS AND APPLICATIONS*. John Wiley & Sons, Inc., 2003.

[21]   J.-R. Li, R. J. Kuppler, and H.-C. Zhou, "Selective gas adsorption and separation in metal-organic frameworks.," *Chemical Society reviews*, vol. 38, no. 5, pp. 1477–504, May 2009.

[22]   R. Staudt and J. Keller, *Gas Adsorption Equilibria, Experimental Methods and Adsorption Isotherms*. Springer Science+ Business Media, Inc., Boston, 2005.

[23]   D. Bradshaw, J. B. Claridge, E. J. Cussen, T. J. Prior, and M. J. Rosseinsky, "Design, chirality, and flexibility in nanoporous molecule-based materials.," *Accounts of chemical research*, vol. 38, no. 4, pp. 273–82, Apr. 2005.

[24]   S. Bourrelly, P. L. Llewellyn, C. Serre, F. Millange, T. Loiseau, and G. Férey, "Different adsorption behaviors of methane and carbon dioxide in the isotypic nanoporous metal terephthalates MIL-53 and MIL-47.," *Journal of the American Chemical Society*, vol. 127, no. 39, pp. 13519–21, Oct. 2005.

[25]   Y. Bae, K. L. Mulfort, H. Frost, P. Ryan, S. Punnathanam, L. J. Broadbelt, J. T. Hupp, and R. Q. Snurr, "Separation of CO 2 from CH 4 Using Mixed-Ligand Metal-Organic Frameworks," *Langmuir*, no. 18, pp. 8592–8598, 2008.

[26]   and J.-M. T. Gerard Ferey, Franck Millange, Mathieu Morcrette, Christian Serre, Marie-Liesse Doublet, Jean-Marc Greneche, "Mixed-Valence Li/Fe-Based Metal–Organic Frameworks with Both Reversible Redox and Sorption Properties," *Angew. Chem. Int. Ed.*, vol. 46, pp. 3259 –3263, 2007.

[27]   G. Hoogers, *FUEL CELL TECHNOLOGY HANDBOOK*. CRC Press LLC, 2003.

[28]   E. Proietti, F. Jaouen, M. Lefèvre, N. Larouche, J. Tian, J. Herranz, and J.-P. Dodelet, "Iron-based cathode catalyst with enhanced power density in polymer electrolyte membrane fuel cells.," *Nature communications*, vol. 2, p. 416, Jan. 2011.

[29]   P. Horcajada, C. Serre, M. Vallet-Regí, M. Sebban, F. Taulelle, and G. Férey, "Metal-organic frameworks as efficient materials for drug delivery.," *Angewandte Chemie (International ed. in English)*, vol. 45, no. 36. pp. 5974–8, 11-Sep-2006.

[30]   W. J. Rieter, K. M. Pott, K. M. L. Taylor, and W. Lin, "Nanoscale coordination polymers for platinum-based anticancer drug delivery.," *Journal of the American Chemical Society*, vol. 130, no. 35, pp. 11584–5, Sep. 2008.

[31]   M. Fleck and L. Bohatý, "Two novel glycine metal halogenides: catena-poly[[[diaquanickel(II)]-di-mu-glycine] dibromide] and catena-poly[[[tetraaquamagnesium(II)]-mu-glycine] dichloride].," *Acta crystallographica. Section C, Crystal structure communications*, vol. 61, no. Pt 9, pp. m412–6, Sep. 2005.

[32]   Y. O. . Toshio Takayama, Shirabe Ohuchida, Yoshio Koike, Masanobu Watanabe, Daisuke Hashizume, "Structural Analysis of Cadmium–Glycylglycine Complexes Studied by X-Ray Diffraction and High Resolution _sup_113__sup_Cd and _sup_13__sup_C Solid State NMR," *Bulletin of the Chemical Society of Japan*, vol. 69, no. 6, p. 1579, 1996.

[33]   C. Martí-Gastaldo, J. E. Warren, K. C. Stylianou, N. L. O. Flack, and M. J. Rosseinsky, "Enhanced stability in rigid peptide-based porous materials.," *Angewandte Chemie (International ed. in English)*, vol. 51, no. 44, pp. 11044–8, Oct. 2012.

[34]   H.-Y. Lee, J. W. Kampf, K. S. Park, and E. N. G. Marsh, "Covalent Metal–Peptide Framework Compounds That Extend in One and Two Dimensions," *Crystal Growth & Design*, vol. 8, no. 1, pp. 296–303, Jan. 2008.

[35]   J. Rabone, Y.-F. Yue, S. Y. Chong, K. C. Stylianou, J. Bacsa, D. Bradshaw, G. R. Darling, N. G. Berry, Y. Z. Khimyak, a Y. Ganin, P. Wiper, J. B. Claridge, and M. J. Rosseinsky, "An adaptable peptide-based porous material.," *Science (New York, N.Y.)*, vol. 329, no. 5995, pp. 1053–7, Aug. 2010.

[36]   R. Ferrari, S. Berne, C. R. De Barbarı, and G. Mendoza-dı, "Interaction between Glyglu and Ca 2 ' , Pb 2 ' , Cd 2 ' and Zn 2 ' in solid state and aqueous solution . Crystal structures of poly [aqua-1 , 2-k-O-di [lead (gly- gluH)] bis (perchlorate)] and poly [bisglycylglutamic-cadmium (II) tetrahydrat," *Inorganica Chimica Acta*, vol. 339, p. 193, 2002.

[37]   D. Bousquet, F. Coudert, A. G. J. Fossati, A. V Neimark, A. H. Fuchs, and A. Boutin, "Adsorption induced transitions in soft porous crystals : An osmotic potential approach to multistability and intermediate structures," *The Journal of Chemical Physics*, vol. 174706, pp. 1–9, 2013.

[38]   J. Zhang, H. Wu, T. J. Emge, and J. Li, "A flexible MMOF exhibiting high selectivity for CO(2) over N(2), CH(4) and other small gases.," *Chemical communications (Cambridge, England)*, vol. 46, no. 48, p. 9152, Dec. 2010.

[39]   D. Seader and E. J. Henley, *SEPARATION PROCESS PRINCIPLES*, Second. John Wiley & Sons, Inc., 2006.